A Toolbox of Subarrays for Optimizing Wide-Angular Scanning Arrays Using Trade-Offs Between Scan Loss and Side Lobe Level

FANNUSH S. AKBAR[ID]**1, (Student Member, IEEE), L. P. LIGTHART**[ID]**2, (Life Fellow, IEEE), AND GAMANTYO HENDRANTORO**[ID]**1, (Senior Member, IEEE)**

[1]Department of Electrical Engineering, Institut Teknologi Sepuluh Nopember, Surabaya 60111, Indonesia
[2]Faculty of Electrical Engineering, Mathematics and Computer Science, Delft University of Technology, 2628 CD Delft, The Netherlands

Corresponding author: Gamantyo Hendrantoro (gamantyo@ee.its.ac.id)

ABSTRACT A novel approach is proposed for building a planar array derived from linear arrays using a toolbox of different types of subarrays located parallel and perpendicular to the linear array axes. The array design assumes constant element patterns and focuses on rectangular array applications with one dimensional, wide-angular beam scanning. Optimization criteria concern a trade-off between side lobe level performance, directive gain scan-loss, reducing the number of element controls and maximizing the use of phase-only elements for beam steering. All subarray configurations and functionalities, for improving the full array performance in sidelobe level and scan-loss compensation, are analyzed and validated in detail. The step-by-step integration of different subarrays starts from the center part of the array. This center part is a linear subarray along the major axis of the rectangular array with uniform maximum amplitude and spatially stretched. This subarray is combined with cross-line subarrays perpendicular to this center axis. At both edges of the center array, two in-line, uniform-amplitude and stretched subarrays are added and combined with cross-line subarrays. The amplitude distribution of the 3 in-line subarrays and the cross-line subarrays allows for lowering the sidelobe level in the plane of scanning. Finally, at both ends of the three in-line subarrays, subarrays with two and five elements are applied for reducing the scan-loss. By assuming $cos(\vartheta)$ element pattern results are given for a planar rectangular array with 41 elements length and 3 elements width. To lower cost and higher power efficiency, the array uses only 33 multi-bit phase shifters, 12 1-bit phase switches, and 4 attenuators for amplitude control. Optimized broadside and 60° scanning patterns are compared and show improved performance in directive gain $D = 24.4$ dBi (broadside), $D = 19.9$ dBi (60°) and in SLL $= -21.6$ dB (broadside), SLL $= -19.5$ dB (60°).

INDEX TERMS Subarray, scanning, scan-loss compensation, sidelobe level.

I. INTRODUCTION

In radar applications that require scanning over a wide angular span, arrays capable of maintaining favorable patterns over the whole scanning field are desired. In such arrays, a large number of elements are necessary to achieve sufficient angle resolution and, accordingly, fewer element controls are often desired to reduce the cost. In the last decade, many research endeavors to reduce the number of element controls in an array while maintaining the side lobe level (SLL) low have relied on solutions that involve thinned non-uniform

The associate editor coordinating the review of this manuscript and approving it for publication was Giorgio Montisci[ID].

arrays [1]–[8]. Particular attention was paid to array pattern synthesis by using a deterministic approach [9]–[16], statistic or heuristic approach by natural algorithm [17], mathematical approach [18], [19], as well as quasi brute force method by evaluating all possible combinations [20]–[22]. Synthesis results have subsequently been applied in more recent years to designs of planar and linear arrays [23]–[33].

Most thinned array pattern syntheses have focused on lowering SLL in the broadside pattern while minimizing the number of elements, which needs precise element locations and amplitude control. However, when wide angular scanning is concerned, the SLL requirements lead to an array design with more elements and with a precise element amplitude

and phase steering. It implies that in wide-angular scanning applications, e.g., up to 60° scanning, nearly no reduction in the number of antenna elements is obtained and that in general the peak SLL (PSLL) becomes worse. This high SLL occurs because the desired main lobe and the side lobes are strongly affected by the element pattern at maximum scan angle of 60°. In addition, the scan loss in directive gain due to the element pattern can be substantial. It is obvious that there is still a gap in realizing an array design for wide-angular scanning applications with an optimized pattern over the scanning angular span and requiring a small number of element controls.

The use of subarrays for various purposes in an array structure has been discussed in many articles [34]–[37]. In our previous works [38]–[40], it has been proven that subarrays with an optimized pattern can increase the scan loss compensation (SLC) and mitigate the PSLL of wide-angular scanning linear arrays. Our previous approach starts from thinning a dense linear array to produce as much empty space as possible. The empty space is subsequently used to accommodate subarrays. The final array configuration is still a linear array due to the use of subarrays with elements located along the linear array axis.

This article promotes a general improvement in the pattern optimization process of planar arrays. It demonstrates novel theoretical and experimental results in the case of a planar array with a length of 41 elements and a width of 3 elements. The array has a wide-angular scanning capability of ±60° along the length axis of the array (x-axis). The width of the array is for increasing the directive gain and allows, at the same time, for amplitude tapering over the length of the array.

In particular, we propose a novel idea of developing a toolbox of subarrays, each with its own structure, feeding, position in the full array and purposes, ready for use in designing a wide-scanning planar array with specified performance criteria that include high directive gain, low scan loss, low sidelobes and small number of controls. The proposed toolbox involves subarrays, oriented either in-line (parallel to the array length) or cross-line (perpendicular to the length), for constructing the planar array antenna. A detailed discussion of the subarrays is given in the following sections, which consists of in-line subarrays of two elements (Type 1), in-line subarrays of three elements (Type 2), in-line subarrays of five elements realized by overlapping two identical three-element subarrays of Type 2, cross-line subarrays of three elements (Type 3) and in-line subarrays with non-uniform element spacing through spatial tapering (Type 4). While subarrays of Types 1 and 2 play the key role in optimizing the SLC and SLL, the Type 3 subarrays are used to adjust the array directive gain and to narrow the elevation beam, whereas the spatially-tapered Type 4 subarrays have the function to imitate Taylor amplitude tapering for suppressing higher sidelobes. The scan loss is analyzed by accounting the effect on directivity due to mutual coupling between the realized Cavity-backed U-slotted Patch (CUP) antenna elements. The element patterns are approximated by a $cos(\vartheta)$-function.

Special attention is paid on analytical expression for calculating the array directive gain after integration of all predefined subarray patterns.

The step-by-step integration of subarrays into the planar array is detailed in a later section, but our array design strategy in brief is as follows. In the center part of the array configuration, spatial stretching along the x-axis at two different amplitude levels is used. This is achieved by employing two different types of subarrays, Type 4a and 4b, in the center part, both of which use phase steering only. By spatial tapering in the center part, a preferred Taylor amplitude tapering distribution over this part of the array can be obtained while destroying periodicity in the element spacing. There is a matching layer at both edges of the center part, which consists of a subarray with a small number of elements belonging to Type 4c. This subarray extends the length of the array center and uses amplitude and phase control in order to obtain low SLL in the scanning plane for all scan angles. The three-element cross-line subarrays (Type 3) are only used on places in the array where extra amplitude control along the array length is needed. In addition, the integration of subarrays of this type also increases the directive gain of the full array and limits the beam width in the elevation plane. The subarrays with two and five elements (Types 1 and 2b, respectively) at both ends of the array configuration are added for pattern adjustment at all scan angles and allow for a trade-off between the SLL and SLC performances.

This article consists of five sections. In Section II, the toolbox of the proposed subarrays configurations is introduced, and their respective general radiation characteristics are discussed. Each proposed subarray is examined and validated in Section III. Section IV presents the step-by-step integration of all examined subarrays to produce a planar array with a low SLL and low scan-loss. Finally, the conclusions are given in the last section.

II. FUNDAMENTALS OF SUBARRAYS FOR BUILDING INTEGRATED SUBARRAYS

As said in Section I, this article is focused on the toolbox of subarrays for use in wide-angular scanning planar arrays allowing for a trade-off between 3 major array qualifiers: the overall directive array gain, the PSLL in the array patterns and scan loss at maximum scan angle, with a constraint of having as few control elements as possible. Such a compromise can only be realized if we have a good design of the array center part together with detailed knowledge on each subarray function in the full array. Maximum flexibility can be obtained when a large part of the full array is composed of different types of subarrays. We aim that the full planar array is completely built up from subarrays.

When designing a planar array consisting of many subarrays, it is of prime importance to specify the subarray locations in the planar array uniquely. In the following paragraph, we present a generalized set up for the planar array and define the Cartesian and Spherical coordinate systems as shown in Fig. 1. It shows that all isolated (that is, non-subarray)
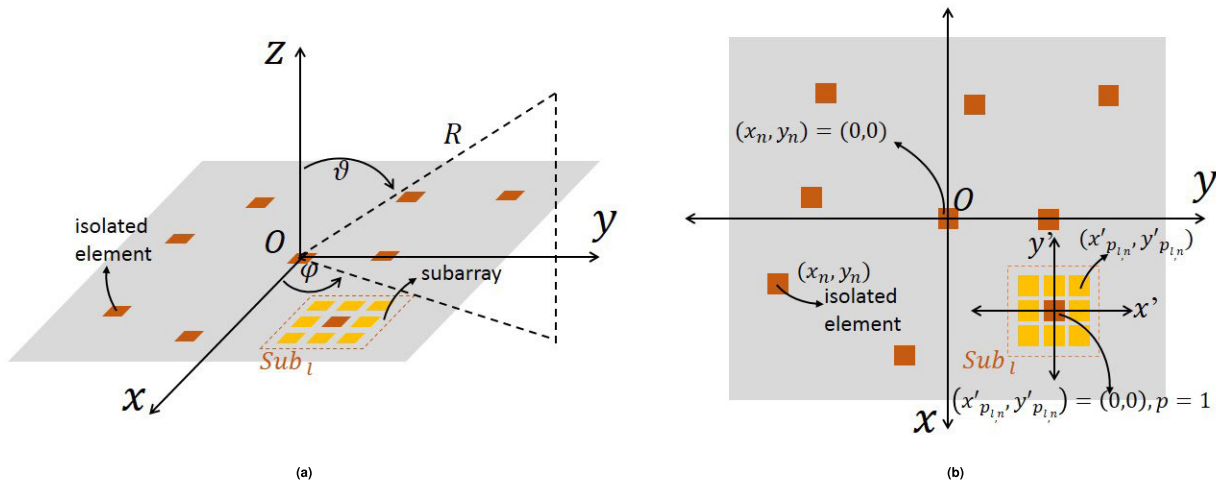
FIGURE 1. The coordinate systems. (a) 3D view; (b) 2D view.

elements in the planar array and all subarray elements are in the *xy*-plane. Elements in a subarray with individual control are isolated elements. Subarrays with center feeding control have center elements at the location of the center feeding and in the subarrays we get non-isolated elements. We assume that the total number of the isolated and the center elements of subarrays equals N. The number of isolated elements and that of subarrays are $N - L$ and L, respectively.

The location of the *n*-th isolated element ($n \leq N - L$) is determined by the x_n and y_n coordinates. Each of such elements has its amplitude and phase that contribute to a scanned beam at the direction of ϑ_0 and φ_0. The radiation is evaluated over the upper half-space only. The *l*-th subarray consists of P_l elements and has its 'local' coordinate system denoted by (x', y'). The (x, y) location of the center element of the subarray coincides with the location of the *n*-th element ($n > N - L$) in the planar array. In Fig. 1b, the coordinates of subarray element p_l are indicated in the 'local' coordinate system.

We assume a rotationally symmetric radiation pattern, which well represents that of a CUP antenna [39] used later in our subarray demonstrator, for all array elements and that the subarray pattern may be non-rotationally symmetric. The basic expression for directive gain of such an array consisting of subarrays is derived in Appendix starting from previous results [41], [42]. In the following, the pattern of each subarray is given, which can then be substituted into equation (A.1) to obtain the directive gain of the full array.

The toolbox provides different subarray configurations needed for realizing the required full array pattern specifications such as directive gain, PSLL and scan loss. There are four types of subarray configurations that are discussed in the following, each having its functionality in the construction of the full array.

The first type of subarray configuration (Type 1, Subsection IIA) has two elements located parallel to the *x*-axis, i.e., in-line, where the input feeding of the subarray is located

at the center between these elements. The second type (Subsection IIB) consists of two configurations; the first one is with three in-line elements (Type 2a), where the input feeding is located at the center element. The other configuration (Type 2b) comprises two overlapped subarrays of Type 2a placed side by side, where the right-side element of the left subarray is overlapped with the left side element of the right subarray. The resulting overlapped subarray has five in-line elements with two input feeding located at subarray elements 2 and 4. The third type (Type 3, Subsection IIC) contains three elements located parallel to the *y*-axis, i.e., cross-line, where the input feeding of the subarray is located at the center element. The last type (Type 4, Subsection IID) has an arbitrary number of in-line elements, each having its own phase shifter. For any type of these subarrays, the input feeding location determines the location of the element in the full array. A detailed example will be given for an extension of a linear array incorporating various subarrays in Section IV.

A. SUBARRAY TYPE 1 (2-ELEMENT IN-lINe SUBARRAY)
The first type of subarray in the toolbox is subarray Type 1, which contributes to scan-loss compensation and keeping low SLL in the full array pattern in the $\varphi = 0°$-plane. It consists of two elements ($P_{1,n} = 2$) and located along the x'-axis, which is parallel to the *x*-axis, as shown in Fig. 2. The elements are separated by a certain spacing and located at $x'_{1_{1,n}}$ and $x'_{2_{1,n}}$ where n is the numbering of the fed antenna elements in the full array, and in this case is equal to $n^{(1)}$ for subarray Type 1. Both elements are fed via a 3 dB power divider (equal power for the two elements). The phase center of this subarray is located precisely at the center between the two elements and coincident with the location of the subarray in the full array characterized by the $x - y$ coordinates. Each element is given an extra phase shift, $\psi_{P1,n}^{(1)}$, to produce high-pattern values as a function of ϑ around the direction of scanning at ϑ_0 for compensating the scan-loss, while low-pattern values

may be realized in other ϑ directions far away from ϑ_0 for suppressing high SLL in those ϑ regions. When the antenna array is to be scanned to the opposite direction with respect to the broadside, this extra phase shift factor is set to its opposite, which can be realized by a 1-bit phase shifter located at the input of each subarray element. This subarray can be positioned when there are empty spaces in that part of the array or can also be considered as an extension at the edges of a linear or planar array. The pattern of the 2-element subarray, $E_1(\vartheta, \varphi, \vartheta_0, \varphi_0)$, can be formulated as,

$$E_{1,n}(\vartheta, \varphi, \vartheta_0, \varphi_0) = cos(\vartheta) \sum_{p_{1,n}=1}^{2} B_{p_{1,n}}^{(1)}$$
$$\times exp\left[j\left(\beta_0 x'_{p_{1,n}} sin(\vartheta)cos(\varphi) + \psi_{p_{1,n}}^{(1)} \right) \right] \quad (1)$$

where the cosine theta function in front of the series indicates the element pattern. The two terms in the series correspond to the two elements in this subarray, where $B_{p_{1,n}}^{(1)}$ and $x'_{p_{1,n}}$ denote the amplitude and location of the $p_{1,n}$-th element, respectively, and $B_{p_{1,n}}^{(1)} = \sqrt{0.5}$. These values, together with the extra phase shift factor applied to both elements, $\psi_{p_{1,n}}^{(1)}$, need to be optimized to produce a desired subarray pattern for compensating scan loss while taking the SLL in the scanning pattern into account. The phases $\psi_{p_{1,n}}^{(1)}$ of subarray elements for $p_{1,n} = 1$ and 2 have positive and negative values, respectively, and the opposite when scanning to negative ϑ_0 angles. When this subarray is integrated in the full array, the formulation becomes,

$$E_{1,n}(\vartheta, \varphi, \vartheta_0, \varphi_0)$$
$$= A_n cos(\vartheta)exp\left[j\left(\xi_n(\vartheta, \varphi) + q_n(\vartheta_0, \varphi_0) \right) \right]$$
$$\times \sum_{p_{1,n}=1}^{2} B_{p_{1,n}}^{(1)} exp\left[j\left(\beta_0 x'_{p_{1,n}} sin(\vartheta)cos(\varphi) + \psi_{p_{1,n}}^{(1)} \right) \right] \quad (2)$$

where $n = n^{(1)}$, since the subarray is placed and fed at the position of the $n^{(1)}$-th element in the full array. It can be seen that the subarray integration into the full array results in an additional factor in front of the series indicated in (1). The factor is related to the $n^{(1)}$-th element in the full array substituted with subarray Type 1. The center of the two-element subarray is at (x_n, y_n), while the phase center is adjusted by a phase shifter value q_n and the center feeding amplitude equals A_n.

The structure shown in Fig. 2 also indicates that a subarray Type 1 can reduce the required number of feeding ports when it is integrated into the full array by occupying two element positions. Accordingly, while the full array requires two feeds for the two original elements, the subarray only requires one feed with a less expense of a power divider and two additional 1-bit phase switches.

B. SUBARRAY TYPE 2 (3-ELEMENT IN-lINe SUBARRAY)
Subarray Type 2 takes one out of two configurations, namely Type 2a and 2b, that have three and five elements, respectively, located along the x'-axis. The Type 2b subarray is arranged from two overlapped subarrays of Type 2a. Both
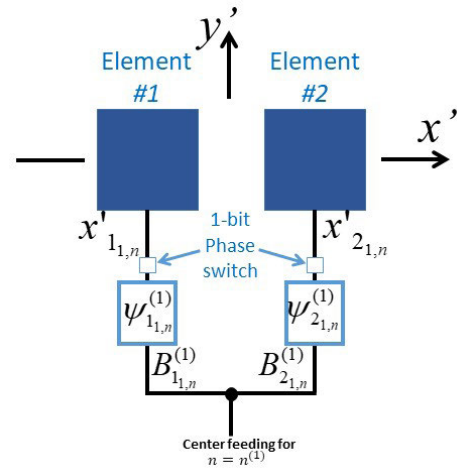

FIGURE 2. Two-element in-line subarray configuration (Subarray Type 1). Subarray elements are located at $x'_{P_{1,n}}$ and fed with complex excitations determined by amplitudes $B_{P_{1,n}}^{(1)}$, and phases $\psi_{P_{1,n}}^{(1)}$.
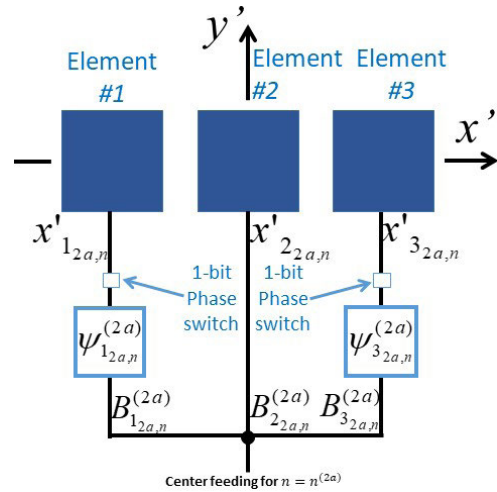

FIGURE 3. Three-element in-line subarray configuration (Subarray Type 2a). Subarray elements are located at $x'_{P_{2a,n}}$ and fed with complex excitations determined by amplitudes $B_{P_{2a,n}}^{(2a)}$, and phases $\psi_{P_{2a,n}}^{(2a)}$.

configurations serve to lower the scan-loss and keeping a low SLL opposite the scan direction, in effect contributing to the array optimization by using only phase controls (along with the other subarrays in the toolbox), which is a novelty on its own. The details of the two configurations are discussed in the following subsections.

1) SUBARRAY TYPE 2a
The 3-element subarray ($P_{2a,n} = 3$) also contributes to scan-loss compensation in the full array pattern on the $\varphi = 0°$-plane. All elements are located along the x'-axis, parallel to the x-axis of the full planar array. The configuration is presented in Fig. 3, in which the center element is located at $x'_{2_{2a,n}}$; this location should coincide with the subarray feeding location in the full array, given in the $x - y$ coordinates. The

two remaining subarray elements are located at $x'_{1_{2a,n}}$ and $x'_{3_{2a,n}}$. For this subarray, n is a specific value $n = n^{(2a)}$ in the numbering of the fed antenna elements in the full array. A 3-way symmetric power divider is used to feed each element with certain amplitude, where the left and right elements are given equal amplitudes. In addition, these elements are given extra asymmetric phase shift factors, with respect to the center element. The extra phase shifts allow for producing high-pattern values at ϑ around scanning angle ϑ_0 to compensate the scan-loss and for producing low-pattern values at the ϑ angles far from scanning angle ϑ_0 to limit SLL in that angular region. When the antenna is scanned to the opposite direction, the extra phase shift shall change to opposite values by implementing a 1-bit phase shifter located at the input of the outer elements in the 3 elements subarrays. For the integration of this subarray in the full array, empty spaces are needed in the original array prior to the addition of subarrays. Alternatively, the subarray can also be used as an extension in linear or planar arrays. The pattern of the three-elements in-line subarray becomes,

$$E_{2a,n}(\vartheta, \varphi, \vartheta_0, \varphi_0) = cos(\vartheta) \sum_{p_{2a,n}=1}^{3} B_{p_{2a,n}}^{(2a)}$$
$$\times exp\left[j\left(\beta_0 x'_{p_{2a,n}} sin(\vartheta)cos(\varphi) + \psi_{p_{2a,n}}^{(2a)}\right)\right] \quad (3)$$

where $B_{p_{2a,n}}^{(2a)}$, $x'_{p_{2a,n}}$, and $\psi_{p_{2a,n}}^{(2a)}$ are the amplitude, location, and the extra phase shift factor of the $p_{2a,n}$-th element, respectively, for $p_{2a,n} = 1, 2$, and 3. As can be seen in Fig. 3, three amplitudes, two phases and two locations need to be optimized to improve SLC and keep SLL low. When this subarray is integrated in the full array, the formulation in (3) becomes,

$$E_{2a,n}(\vartheta, \varphi, \vartheta_0, \varphi_0)$$
$$= A_n cos(\vartheta)exp\left[j\left(\xi_n(\vartheta, \varphi) + q_n(\vartheta_0, \varphi_0)\right)\right]$$
$$\times \sum_{p_{2a,n}=1}^{3} B_{p_{2a,n}}^{(2a)} exp\left[j\left(\beta_0 x'_{p_{2a,n}} sin(\vartheta)cos(\varphi) + \psi_{p_{2a,n}}^{(2a)}\right)\right]$$
$$(4)$$

where $n = n^{(2a)}$, denoting that the subarray has one input at the $n^{(2a)}$-th element location in the full array. The center element is located at (x_n, y_n), which also indicates the phase center of the subarray that is adjusted by a phase shifter value q_n while the center amplitude equals A_n.

Fig. 3 shows that when a subarray Type 2a is integrated into the full array, it occupies three element positions and reduces the requirement for feeding ports from three into one, with a mere consequence of adding a 3-way power divider two 1-bit phase switches.

2) SUBARRAY TYPE 2b
The more advanced configuration with improved array pattern performance (on scan loss and SLL) is obtained by combining in a special way two identical 3-element subarrays
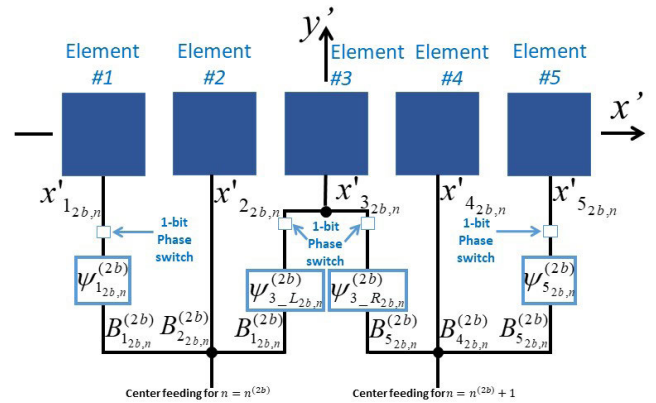

FIGURE 4. Overlapped two sets of 3-elements in-line subarrays resulting into a 5-element subarray configuration (Subarray Type 2b). Subarray elements are located at $x'_{p_{2b,n}}$ and fed with complex excitations determined by amplitudes $B_{p_{2b,n}}^{(2b)}$, and phases $\psi_{p_{2b,n}}^{(2b)}$.

of Type 2a placed next to each other. The special combination has been realized by overlapping the neighboring side elements of the subarrays. By doing so, the combination of two 3-element subarrays results in a subarray with 5 elements, instead of 6 elements. The overlapped subarrays configuration is shown in Fig. 4, in which the overlapped element is located at $x'_{3_{2b,n}}$. The 5-elements subarray has two feeding inputs located at $x'_{2_{2b,n}}$ and $x'_{4_{2b,n}}$. These inputs occupy two locations in the full array given in $x - y$ coordinates. Both inputs are fed via the same type of phase shifters as used for the isolated array elements in the original array.

The leftmost element of the subarray is located at $x'_{1_{2b,n}}$, while the rightmost is at $x'_{5_{2b,n}}$. Similar to the treatment to the side elements of subarray Type 2a, the elements at $x'_{1_{2b,n}}$ and $x'_{5_{2b,n}}$ are given extra (1-bit) phase shift factors, with respect to elements at $x'_{2_{2b,n}}$ and $x'_{4_{2b,n}}$, respectively, to produce a scanned subarray pattern with lower scan loss. The overlapped element, located at $x'_{3_{2b,n}}$, is affected by the phases of the elements located at $x'_{2_{2b,n}}$ and $x'_{4_{2b,n}}$. The pattern of this subarray strongly affects the pattern of the full array, particularly when the antenna pattern is scanned to large ϑ_0 scan angles for $\varphi = 0°$. This subarray can be used when large empty areas in the array are available; otherwise it should be integrated at the edges of the array configuration. The radiation pattern of the extended version of Subarray Type 2a, $E_{2b,n}(\vartheta, \varphi)$, is formulated as,

$$E_{2b,n}(\vartheta, \varphi, \vartheta_0, \varphi_0)$$
$$= cos(\vartheta) \sum_{n=n^{(2b)}}^{n^{(2b)}+1} A_n exp\left[j\left(\xi_n(\vartheta, \varphi) + q_n(\vartheta_0, \varphi_0)\right)\right]$$
$$\times \sum_{p_{2b,n}=1}^{3} B_{p_{2b,n}}^{(2b)} exp\left[j\left(\beta_0 x'_{p_{2b,n}} sin(\vartheta)cos(\varphi) + \psi_{p_{2b,n}}^{(2b)}\right)\right]$$
$$(5)$$

The first series corresponds to complex excitation, i.e., amplitude A_n and phase q_n, of two specific full array

locations coinciding with two isolated elements, i.e., $n^{(2b)}$ and $n^{(2b)} + 1$, in the full array. The second series represents the three-elements subarray Type 2a as given before. However, in this case, $x_{n^{(2b)}}$ and $x_{n^{(2b)}+1}$ has a λ spacing. It leads to coinciding elements at $x'_{3_{2b,n^{(2b)}}}$ and $x'_{1_{2b,n^{(2b)}}}$, which in turn results in a five-elements array with coinciding element in the local origin. Therefore, (5) becomes,

$$E_{2b,n}(\vartheta, \varphi, \vartheta_0, \varphi_0) = cos(\vartheta) \sum_{p_{2b,n}=1}^{5} B_{p_{2b,n}}^{(2b)}$$
$$\times exp\left[j\left(\beta_0 x'_{p_{2b,n}} sin(\vartheta)cos(\varphi) + \psi_{p_{2b,n}}^{(2b)}\right)\right] \quad (6)$$

In (6), $B_{p_{2b,n}}^{(2b)}$ and $\psi_{p_{2b,n}}^{(2b)}$ are the amplitude and the extra phase shift of the $p_{2b,n}$-th element of the Type 2b subarray, which, like in the case of the Type 2a, need to be optimized in order to produce a subarray pattern for compensating scan loss and limiting SLL degradation. The cosine theta function in front of the series represent the element pattern. Due to the identical 3-element subarrays which are overlapped in the middle, we obtain $B_1^{(2b)} = B_5^{(2b)}$. Meanwhile, the complex amplitude of the overlapped element, $B_3^{(2b)}$, is determined by,

$$B_3^{(2b)} = B_1^{(2b)} \left\{ exp\left[j\left(\psi_{3\_L}^{(2b)}\right)\right] + exp\left[j\left(\psi_{3\_R}^{(2b)}\right)\right] \right\} \quad (7)$$

where $\psi_{3\_L}^{(2b)}$ and $\psi_{3\_R}^{(2b)}$ are the phase feeding of the overlapped elements from the left-side and right-side subarrays, respectively. It can be seen from (7) that the third element ($p_{2b,n} = 3$) obtains the amplitude from the left-side subarray, determined by $B_1^{(2b)}$, and from the right side subarray, determined by $B_5^{(2b)}$. In addition, the middle element gets a phase shift factor, which can be derived from the phase shift factor of the left-side and right-side subarrays. We derive the left-side and right-side subarrays, $-\psi_{3\_L}^{(2b)}$ and $+\psi_{3\_R}^{(2b)}$, respectively, in the case of scanning to a positive angle. Meanwhile, for negative scanning angles, these phases become $+\psi_{3\_L}^{(2b)}$ and $-\psi_{3\_R}^{(2b)}$, respectively. The phase changing is realized by using a 1-bit phase switch at each branch. The combination of these two branches, to feed the third element, is realized by using an equal power combiner. Like subarrays of Type 1 and 2a, this subarray also plays a role of reducing the number of feeding ports from five to two in the expense of additional two 3-way power divider, four 1-bit phase switches and a 2-way power combiner, which in total are still less expensive than using 5 RF modules controlling amplitude and phase.

C. SUBARRAY TYPE 3 (3-ELEMENT CROSS-LINE SUBARRAY)

Subarray Type 3 is used for adjusting the array pattern in the $y - z$ plane ($\varphi = 90°$). The index of the center element is located at the x-axis and coincides with the $n = n^{(3)}$ element in the full array. Meanwhile, the other two subarray elements are located above and below the center element, that is, along the local y'-axis parallel to the y-axis of the full array. In this manner, a planar array with a width of three elements is realized. The index of the center element $n = n^{(3)}$ is a specific
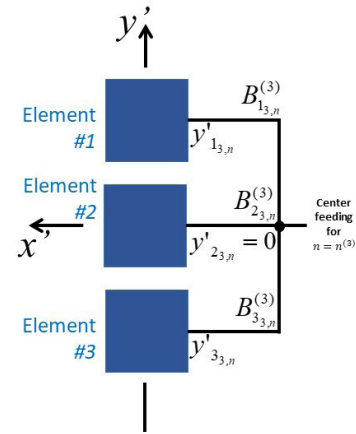

FIGURE 5. Three-element cross-line subarray configuration (Subarray Type 3). All elements are located at *y*-axis and have equal phase feeding using a 1-to-3 power divider. The center element located at $y'_{2_{3,n}}$ corresponds with the location $n = n^{(3)}$ in the full array.

value in the numbering of the fed antenna elements in the full array. In this subsection, we focus on the applicability of this subarray when integrated into a linear array along the *x*-axis. As demonstrated in Section 4, the improved gain and patterns characteristics of a linear array along the *x*-axis are obtained by using in-line and cross-line subarrays. Since scanning is done in the $x - z$ plane, the cross-line subarrays have no scanning duties. However, by integrating the extra cross-line subarray elements, the beamwidth of the elevation pattern perpendicular to the linear array axis becomes narrower. The configuration of this subarray, with $P_{3,n} = 3$, is presented in Fig. 5. The center element is located at $y'_{2_{3,n}} = 0$ which determines the actual element location in the phased array. The other two elements are located at $y'_{1_{3,n}}$ and $y'_{3_{3,n}}$, in the coordinate system of this subarray. The subarray has a symmetric amplitude distribution, and all elements get equal phase feeding. A directive gain increment can be so obtained thanks to these 'extra' elements. For optimizing linear arrays along the *x*-axis, this subarray can be integrated in all parts (especially in the center part) of a linear array. For this non-scanning subarray, the subarray pattern has a ϑ dependence similar to the element $cos(\vartheta)$-pattern. The pattern of the 3-element cross-line subarray, $E_{3,n}(\vartheta, \varphi)$,

$$E_{3,n}(\vartheta, \varphi, \vartheta_0, \varphi_0) = cos(\vartheta) \sum_{p_{3,n}=1}^{3} B_{p_{3,n}}^{(3)}$$
$$\times exp\left[j\beta_0 y'_{p_{3,n}} sin(\vartheta)sin(\varphi)\right] \quad (8)$$

where $B_{p_{3,n}}^{(3)}$ and $y'_{p_{3,n}}$ are the amplitude and element location of the $p_{3,n}$-th element along the *y*-axis. The cosine theta function indicates the element pattern. The amplitudes are realized by a symmetric 1-to-3 power divider, for realizing maximum directive gain and narrower patterns in the plane perpendicular to the array length. However, it should be noted that this type of subarray can also be used for realizing

a lower amplitude value without adding attenuators. Such lower amplitude can be obtained by adjusting the power divider ratio of the output branches while keeping a unit input power. An example of this application will be discussed and presented in the next section.

When this subarray is integrated in the full array, (8) becomes,

$$
\begin{aligned}
E_{3,n}&(\vartheta, \varphi, \vartheta_0, \varphi_0) \\
&= cos(\vartheta)A_n exp\left[j\left(\xi_n(\vartheta, \varphi) + q_n(\vartheta_0, \varphi_0)\right)\right] \\
&\quad \times \sum_{p_{3,n}=1}^{3} B_{p_{3,n}}^{(3)} exp\left[j\left(\beta_0 y'_{p_{3,n}} sin(\vartheta)cos(\varphi)\right)\right]
\end{aligned} \quad (9)
$$

where $n = n^{(3)}$ indicating that the $n^{(3)}$-th element in the full array is substituted by subarray Type 3. The phase center of the subarray is adjusted by a phase shifter value q_n, while the center input amplitude equals A_n.

D. SUBARRAY TYPE 4

The last set of subarrays in our toolbox are those of the Type 4 family, the functionality of which is described as follows. In a linear array with uniform amplitudes and equidistant spacing, a high SLL occurs in wide-angular scanning applications. This high SLL can be suppressed by destroying the periodicity of the inter-element spacing [1]–[33], i.e., by using spatial tapering. From the so-obtained spatial tapering, a virtual specific amplitude tapering can be realized by varying the spacing between successive elements. For example, as part of a Taylor distribution tapering, we can use stretching of the inter-element spacing around the center element of the linear array up to a maximum spacing. The variation from maximum to minimum spacing determines the equivalent variation in amplitude tapering from minimum to maximum amplitude.

Subarray Type 4 is basically a linear array with individual feeding. In-line integration of different Type 4 subarrays (Types 4a, 4b, and 4c) constitutes the linear array with $N - L$ individually fed elements in the 4c-4b-4a-4b'-4c' order, where 4b' and 4c' are the version of 4b and 4c flipped along the x-axis, respectively. Subarrays 4a, 4b, and 4c employ different spatial stretching in such a way that the integration of all subarrays Type 4 creates 'virtual' amplitude tapering that follows the Taylor distribution over the composite linear array consisting of subarrays Types 1, 2, and 4. Furthermore, the integration with Type 3 subarrays will transform the linear array into a planar array. The three subarray Types 4, are summarized in the following subsection.

As indicated, there are limitations for determining the inter-element spacing, the minimum value being equal to the physical antenna size, while the maximum spacing d_{max} relative to wavelength is derived from the constraint to avoid grating lobes in an equidistant scanning array. For maximum scan angle, ϑ_{0_max}, the maximum spacing d_{max} gives the
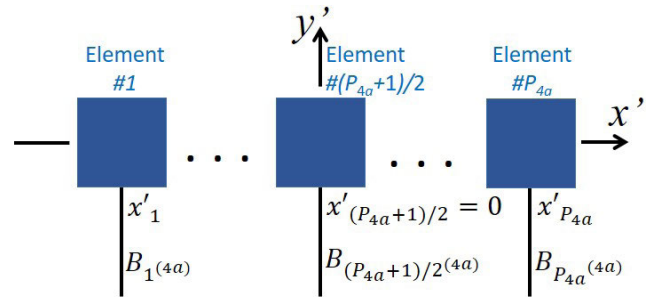

FIGURE 6. Subarray Type 4a, consists of P_{4a} number of elements fed with individual uniform amplitude values and inter-element spacing variation. This subarray is symmetrically located at the center part of the array with maximum uniform amplitude. Each subarray element associated with an isolated element in the full linear array.

lowest value in the virtual amplitude taper where [41],

$$
d_{max}(\vartheta_0) = \frac{1}{1 + (sin(\vartheta_{0\_max}))} \quad (10)
$$

1) SUBARRAY TYPE 4a

Subarray Type 4a is an in-line linear array located at the center part of the full linear array, with spatial tapering that is symmetrical around its center, which coincides with the center of the full array. The subarray represents the dense part of the linear array with individual element feeding of uniform amplitudes, so that only a phase control per element is necessary. It is given phase shift factor per x_n location and per 'isolated' element in the full array, which depends on ϑ_0 and φ_0 when scanning in the xz-plane is considered. This type of subarray, positioned in the center part of the full linear array, also serves to provide one level of spatial tapering. The configuration of subarray Type 4a is shown in Fig. 6. It can be seen that the first element in the local coordinate system is located at $x'_{1_{4a,n}}$, while the last element is located at $x'_{P_{4a,n}}$. The symmetry of its structure implies that $x'_{1_{4a,n}} = -x'_{P_{4a,n}}$ and $x'_{(P_{4a,n}+1)/2} = 0$, assuming the subarray has an odd number of elements. The radiation pattern of this subarray, $E_{4a,n}(\vartheta, \varphi)$, is formulated as,

$$
\begin{aligned}
E_{4a,n}(\vartheta, \varphi, \vartheta_0, \varphi_0) &= A_{n^{(4a)}}cos(\vartheta) \sum_{n=n^{(4a)}}^{n=n^{(4a)}+P_{4a}} B_{n^{(4a)}} \\
&\times exp\left[j\left(\beta_0 x'_{p_{4a}} sin(\vartheta)cos(\varphi) + q_n(\vartheta_0, \varphi_0)\right)\right]
\end{aligned} \quad (11)
$$

where $B_{n^{(4a)}}$ is the amplitude of the n-th element in the subarray Type 4a, which is identical for all elements of the subarray, while $A_{n^{(4a)}}$ is the amplitude of the center element. The element positions along the x'-axis need to be optimized to produce a pattern with lower SLL. Besides that, the origin of the local coordinate system coincides with the origin of the full array. The maximum spacing is already obtained in (10), while the minimum spacing is determined by the physical size of the antenna. It is noted that (11) gives also the subarray pattern because the subarray center coincides with the origin of the coordinate system of the full array.
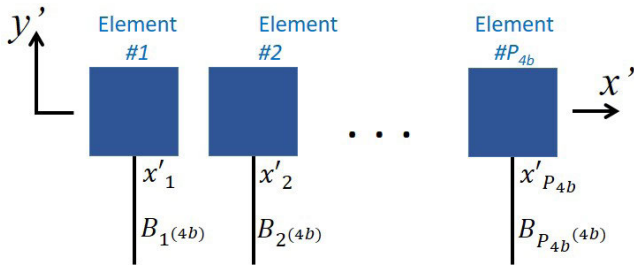
FIGURE 7. Subarray Type 4b consists of P_{4b} number of elements fed with individual uniform amplitude values and inter-element spacing variation. This subarray is located at both the left and right sides of subarray Type 4a, with a lower uniform amplitude realized by the power divider of subarray Type 3 but different power division. The p_{4b}-th element determines an isolated element in the full linear array.

2) SUBARRAY TYPE 4b

As in the case of subarray Type 4a, subarray Type 4b elements have equal amplitudes, and the virtual amplitude tapering comes from varying the spacing between successive elements. The stretched elements are located along the x'-axis, but unlike the Type 4a subarray, the Type 4b subarray is not symmetrical and is positionally shifted relative to the center of the x-axis. In such a way, this subarray can be considered as the left and right extension of subarray Type 4a at the center of the full array to lower the virtual amplitude tapering at both sides of the array; in this way, the resulting virtual amplitude over the combination of Type 4a and 4b subarrays fits better to the Taylor distribution. It means that the element with the maximum virtual amplitude tapering value in subarray Type 4b must 'match' with the element with the minimum virtual amplitude tapering value in subarray Type 4a. For matching the slope of the Taylor distribution, the amplitude transition between these 2 subarrays should be optimally followed. The maximum amplitude in subarray Type 4b is also determined by the spacing between this subarray and subarray Type 4a. The lower amplitude value can be realized by using a power divider with a required power division in the cross-line 3 elements Type 3 subarray. Later in the next section, we show that the different amplitudes between the Type 4a subarray at the center and the Type 4b extensions can be achieved by integrating cross-line subarrays Type 3 with two different directive gains obtained by applying power dividers with different power divisions.

The non-equidistant element locations, along the x-axis, should improve the suppression of the high SLL of the scanned array pattern in the $\varphi = 0°$-plane. The subarray elements are given phase shift factors that are determined by the subarray element locations x_n as part of the 'linear array' elements in the full array and which depend on ϑ_0 and φ_0 when scanning in the xz-plane is considered. Due to the use of equal amplitudes, this subarray requires only phase controls for the elements. The configuration of subarray Type 4b is shown in Fig. 7. The elements are located at $x_n = x'_{p_{4b}}$ in the coordinate systems of the full array and subarray respectively, with $n = n^{(4b)} + p_{4b}$ and $p_{4b} = 1, 2, \ldots, P_{4b}$. The radiation

pattern of this subarray, $E_{4b,n}(\vartheta, \varphi)$, can be expressed as,

$$E_{4b,n}(\vartheta, \varphi, \vartheta_0, \varphi_0) = A_{n^{(4b)}+P_{4b}} cos(\vartheta) \sum_{p_{4b}=1}^{P_{4b}} B_{n^{(4b)}}$$
$$\times exp\left[j\left(\beta_0 x'_{p_{4b}} sin(\vartheta)cos(\varphi) + q_n(\vartheta_0, \varphi_0)\right)\right] \quad (12)$$

where the amplitude and location of the $p_{4b,n}$-th element are indicated by $B_{n^{(4b)}}$ and $x'_{p_{4b}}$, respectively. The amplitude value is uniform for all elements, while the inter-element spacing needs to be optimized to lower SLL. As discussed in the previous subsection, the maximum and minimum spacing is determined by (10) and the physical size of the antenna, respectively. We learned in our analysis with a sufficiently large number of elements (in the order of 20 or more), that it is allowed to have one element, at each side, which has spacing beyond the maximum spacing defined in (10).

3) SUBARRAY TYPE 4c

Subarray Type 4c provides the final amplitude matching over the array along the x-axis by integrating this linear array at the edges of the combination of one linear subarray Type 4a and two linear subarrays Type 4b. This subarray Type 4c consists of P_{4c} elements with amplitude and phase control to obtain the required amplitude taper and phase shift for beam steering. For this array, it is assumed that all elements are located at a $\lambda/2$-grid, along a shifted axis relative to the x-axis. This grid is chosen to avoid high side lobes at ϑ-angles far away from the ϑ_0 angle.

The amplitude function over the outer area of an array is important for realizing a low SLL in the array patterns. When the amplitude function is similar to a required amplitude tapering distribution, i.e. Taylor distribution, low SLL can be obtained in the full array pattern. Therefore, this subarray uses amplitude and phase control at each element to produce a certain tapering value, particularly an amplitude value below 1. The maximum tapering value at each side is derived from the lowest amplitude of subarray Type 4b and from the spacing with subarray Type 4b. This subarray will be the matching part between the subarrays with stretching (Types 4a and 4b) and the edge parts of the full linear array part consisting of subarrays Type 1 and Type 2. All elements are given phase shift factors corresponding to the 'real' element locations in the full array configuration, which depend on ϑ_0 and φ_0 when scanning in the xz-plane is considered. It is shown in Fig. 8 that the first element of subarray Type 4c is located at $x'_{1_{4c}}$, while the last, i.e., P_{4c}-th element is located at $x'_{P_{4c}}$ in the coordinate systems of the full array and subarray respectively, with $n = n^{(4c)} + p_{4c}$ and $p_{4c} = 1, 2, \ldots, P_{4c}$. All elements are fed via attenuators for realizing the targeted amplitude tapering. The radiation pattern of this subarray, $E_{4c,n}(\vartheta, \varphi, \vartheta_0, \varphi_0)$, is formulated as,

$$E_{4c,n}(\vartheta, \varphi, \vartheta_0, \varphi_0) = cos(\vartheta) \sum_{p_{4c}=1}^{P_{4c}} B_{n^{(4c)}}$$
$$\times exp\left[j\left(\beta_0 x'_{p_{4c}} sin(\vartheta)cos(\varphi) q_n(\vartheta_0, \varphi_0)\right)\right] \quad (13)$$

TABLE 1. Recapitulation of subarray types in the toolbox.

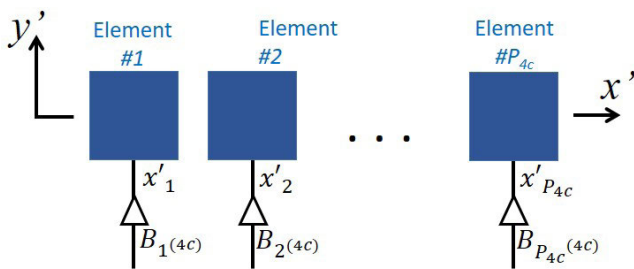| Subarray Type (l)	Number of elements	Subarray pattern $(E_{l,n})$	Feeding scheme	Position in the full array	Objective / Functionality
1	$P_1 = 2$	Eq. (1)	Center feed with a 2-way power divider.	Edge part, in-line, occupying one x_n value. Different sides are mirrored.	Scan loss compensation, side-lobe level suppression, reduction of feeding ports.
2a	$P_{2a} = 3$	Eq. (3)	Center feed with a 3-way power divider.	Edge part, in-line, occupying one x_n value. Different sides are mirrored.	Scan loss compensation, side-lobe level suppression, reduction of feeding ports.
2b	$P_{2b} = 5$	Eq. (5)	Two feeds with two 3-way power dividers for each half and a 2-way equal divider for overlapped third element.	Edge part, in-line, occupying two x_n and x_{n+1} values. Different sides are mirrored.	Scan loss compensation, side-lobe level suppression, reduction of feeding ports.
3	$P_3 = 3$	Eq. (8)	Center feed with a 3-way power divider.	Center part, cross-line. Occupying one x_n value.	Directive gain adjustment without attenuator, narrowing beam on the $\varphi = 90°$ plane.
4a	P_{4a}, odd	Eq. (11)	Individual equal-amplitude element feed with phase shifter.	Center part, in-line, with spatial stretching. Occupying P_{4a} array elements positions. Different sides are mirrored.	Side-lobe level suppresion with uniform amplitude feeds.
4b	P_{4b}	Eq. (12)	Individual equal-amplitude element feed with phase shifter.	Center part, in-line, with spatial stretching, on the left and right sides of 4a with mirrored spacings and feeds. Occupy P_{4b} array elements positions.	Side-lobe level suppresion with uniform amplitude feeds.
4c	P_{4c}, small	Eq. (13)	Individual element feed with phase shifter with/without attenuator.	Center part, in-line, on the left and right sides of the "4b-4a-4b" configuration with mirrored feeds. Occupy P_{4b} array elements positions.	Amplitude matching of adjacent subarrays to obtain a desired amplitude tapering.

FIGURE 8. Subarray Type 4c consists of P_{4c} number of elements fed with individual amplitude via an attenuator and with equidistant spacing. The p_{4c}-th element corresponds with an isolated element located at x_n in the full linear array.

where $B_{n(4c)}$ and $x'_{p_{4c}}$ denote the amplitude and location of the p_{4c}-th element, respectively. The amplitude values need to be optimized to produce a desired subarray pattern for lowering SLL. This subarray also uses asymmetric element location in the local coordinate due to its location as extensions in the left and right sides of subarray Type 4b. In this subarray we have solitary elements with no cross-line elements and each element has a specific amplitude $B_{n(4c)}$.

The toolbox of subarray types and their major characteristics as presented in this article, are summarized in Table 1.

III. SUBARRAY DESIGNS, PATTERN CHARACTERISTICS, AND VALIDATION

A toolbox of subarrays for building a planar array consisting of different types of subarrays with different purposes has been introduced in the previous section. In this section, the actual subarray designs and their pattern and directive gain characteristics are detailed for use in the full array application presented in Section IV. Focus is given to azimuth scanning pattern of subarrays Type 1, 2, 4 and to the non-scanning pattern of subarray Type 3. In the design, a $cos(\vartheta)$ element pattern is used in the array pattern calculations. For subarrays Type 1 and Type 2a, the amplitudes and phases have been determined and validated in our previous article [40]. These values were derived and realized for increasing the SLC and for lowering the SLL in a linear array. For the other subarray types, the amplitudes and phases are optimized for use in the full planar array, presented in Section IV. Therefore in this section the various subarray designs and performances are presented while the realization and experimental validation are conducted only for the subarrays Type 3 with two types of amplitudes configuration. Subarrays Type 4 does not need validations because they are just linear arrays using individual feeding, and their designs can be found in many array handbooks, e.g., [41].
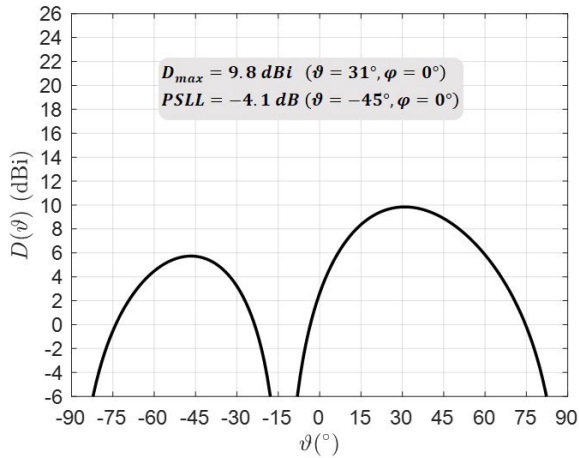
FIGURE 9. Pattern ($\varphi = 0°$) of the subarray Type 1 (2 elements), with $B^{(1)}_{1_{1,n}} = B^{(1)}_{2_{1,n}} = 0.7$, $\psi^{(1)}_{1_{1,n}} = +70°$, $\psi^{(1)}_{2_{1,n}} = -70°$, and $\lambda/2$-grid elements. This subarray pattern is for positive scan angles application, while for the negative scan angles the pattern is just its mirror around broadside.

FIGURE 10. Pattern ($\varphi = 0°$) of the subarray Type 2a (3 elements), with $B^{(2a)}_{2_{2a,n}} = 0.82$, $B^{(2a)}_{1_{2a,n}} = B^{(2a)}_{3_{2a,n}} = 0.41$, $\psi^{(2a)}_{1_{2a,n}} = +140°$, $\psi^{(2a)}_{3_{2a,n}} = -140°$, and $\lambda/2$-grid elements. This subarray pattern is for positive scan angles application, while for the negative scan angles the pattern is just its mirror around broadside.

A. SUBARRAY TYPE 1 (2-ELEMENT IN-lINe SUBARRAY)

Pattern characteristics of Subarray Type 1 will be shown for positive scan angles, using a selected state of the 1-bit phase shifters. The element amplitudes are $B^{(1)}_{P1,n} = [0.7; 0.7]$, while the phases are $\psi^{(1)}_{P1,n} = [+70°; -70°]$ for $p_{1,n} = 1, 2$. These amplitudes and phases are obtained from an equal-split power divider, with a unit input power, and 1-bit phase switches with a certain delay line at each input of each element. The values have been optimized in [40] as a trade-off between SLC and PSLL.

The scanned subarray patterns are plotted in Fig. 9,where the subarray pattern does not depend on the scanning angle. It can be seen that this subarray is not ϑ_0 dependent because there is no phase shifter with ϑ_0 dependence inside the sub-array. From the plot, we can identify a maximum directive gain, $D_{max} = 9.8$ dBi, at $\vartheta = 31°$. In addition, the PSLL is obtained in the negative ϑ direction and is 4.1 dB below the mainlobe level. It means that this subarray is optimum for scanning around $\vartheta = 25°$ up to $\vartheta = 40°$ and the sidelobes at the negative ϑ angles are suppressed. Latter in the full array pattern construction, the maximum part of the subarray pattern is for compensating the scan loss while the other side is for lowering the far sidelobes.

B. SUBARRAY TYPE 2 (3-ELEMENT IN-lINe SUBARRAY)

1) SUBARRAY TYPE 2a

This subarray is again analyzed for positive scan angles. The amplitude for the center element is, $B^{(2a)}_{2_{2a,n}} = 0.82$, while for the left and right sides the amplitudes are equal, $B^{(2a)}_{1_{2a,n}} = B^{(2a)}_{3_{2a,n}} = 0.41$. This amplitude distribution is determined from a symmetric power divider with a unit input power. The phase of the center element is determined by the phase shift factor of the center element in the full array configuration, while for the left and right elements the subarray phase factors relative to the center element are, $\psi^{(2a)}_{1_{2a,n}} = +140°$ and $\psi^{(2a)}_{3_{2a,n}} = -140°$,
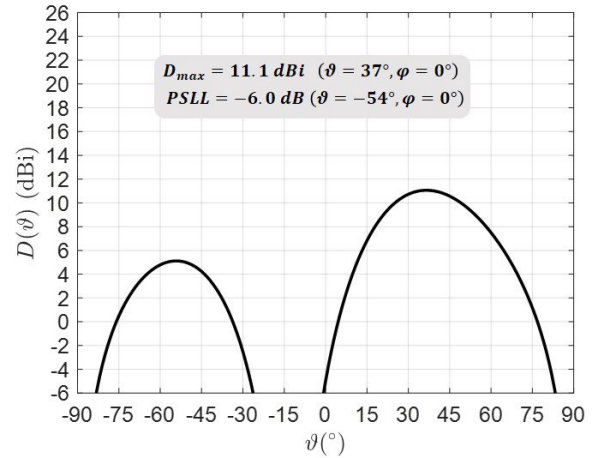
respectively. The amplitudes and phase factors are found from a trade-off between SLC and PSLL [36].

The scanned subarray patterns are plotted in Fig. 10, where the subarray pattern is not depending on the scanning angle. The absence of phase shifters with ϑ_0 dependence inside the subarray implies that this subarray is not ϑ_0 dependent. A maximum directive gain $D_{max} = 11.1$ dBi is obtained at $\vartheta = 35°$, while the PSLL in the negative ϑ direction is 6.0 dB below the main lobe level. This subarray gives an optimum scanning performance from around $\vartheta = 30°$ upto $\vartheta = 45°$, and the sidelobes at negative ϑ angles are suppressed. These indicate that for full array pattern construction, the scan loss can be compensated by the maximum part, while the far side-lobes at the other side can also be obtained. The improvement of D_{max} and PSLL performances are obtained with one extra element compared with the subarray Type 1.

2) SUBARRAY TYPE 2b

The overlapped subarrays (Type 2b) is ϑ_0 dependent because it has two feeding inputs. These two elements are at locations in the full array and get phase shift factors corresponding to the wanted scan angle. The amplitudes are, $B^{(2b)}_{2_{2b,n}} = B^{(2b)}_{4_{2b,n}} = 0.82$ and $B^{(2b)}_{1_{2b,n}} = B^{(2b)}_{5_{2b,n}} = 0.41$, while the phases are (see equation(8)) $\psi^{(2b)}_{1_{2b,n}} = +140°$, $\psi^{(2b)}_{5_{2b,n}} = -140°$, and $\psi^{(2b)}_{3\_L_{2b,n}} = -140°$, $\psi^{(2b)}_{3\_R_{2b,n}} = +140°$, from the left and right sides subarrays, respectively.

The scanned subarray patterns are plotted in Fig. 11. For broadside scanning, the maximum directive gain, D_{max}, of 12.1 dBi is obtained at $\vartheta = 53°$, while, the PSLL of -3.4 dB below the mainlobe level is obtained at $\vartheta = -60°$. For broadside scanning, both the maximum directive gain and the high sidelobe are not desired, but they have limited effect in the full array pattern when scanned to broadside direction because these lobes are far away from broadside and naturally suppressed by the full array and the element patterns. For 30°
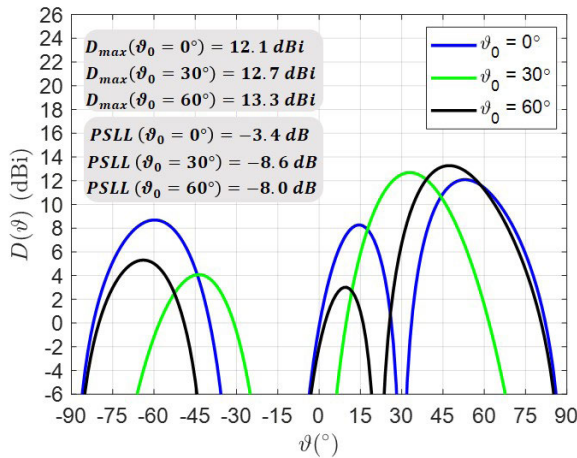
FIGURE 11. Pattern ($\varphi = 0°$) of the subarray Type 2b (5 elements), with $B_{2_{2b,n}}^{(2b)} = B_{4_{2b,n}}^{(2b)} = 0.82$, $B_{1_{2b,n}}^{(2b)} = B_{5_{2b,n}}^{(2b)} = 0.41$, $\psi_{1_{2b,n}}^{(2b)} = +140°$, $\psi_{3\_L_{2b,n}}^{(2b)} = -140°$, $\psi_{3\_R_{2b,n}}^{(2b)} = +140°$, $\psi_{5_{2b,n}}^{(2b)} = -140°$, and $\lambda/2$-grid elements. The patterns are for positive scan angles, $\vartheta_0 = 0°$, +30°, and +60°.

FIGURE 12. Elevation pattern ($\varphi = 90°$) of the subarray Type 3 (3 elements parallel to *y*-axis), with $B_{P3,n}^{(3)} = [0.505; 0.7; 0.505]$ and $\lambda/2$-grid elements. This subarray pattern is not ϑ_0 dependent.

scanning, a 12.7 dBi directive gain, D_{max}, is obtained at $\vartheta = 30°$, while for the PSLL of 8.6 dB below the main lobe level is obtained at $\vartheta = -43°$. For 60° scanning, a 13.3 dBi directive gain, D_{max}, is obtained at $\vartheta = 60°$, while the PSLL of 8.0 dB below the main lobe level is obtained at $\vartheta = -63°$. The results for 30° and 60° scanning angles indicate that the full array pattern exhibits a high gain at the direction of scanning and good sidelobe suppression in the other directions. From the analysis of the scanned patterns, it can be concluded that this overlapped subarray with five elements is promising to compensate the scan loss in the full array pattern, especially in the 30° scanning where it has the highest directive gain.

C. SUBARRAY TYPE 3 (3-ELEMENT CROSS-LINE SUBARRAY)

In this article, there are two configurations realized using the same Type 3 subarray structure by applying different sets of amplitudes for two different objectives. The first configuration, referred to herein as Type 3a, is used to enhance the directive gain without adding T/R modules and adjusting the elevation pattern, whereas the second, called Type 3b, primarily seeks to lower the amplitudes over the full array without additional attenuators. It is immediately obvious that these two configurations can be beneficial to realize a two-step virtual amplitude tapering by employing the first at the center of the full array and the second on the left and right of the center subarray.

In Type 3a, the amplitude values of $B_{p3,n}^{(3)} = [0.505; 0.7; 0.505]$ are used. These values are chosen because the corresponding subarray pattern has a narrow elevation beamwidth while keeping a unit input power, but the elevation beamwidth is not the main subject in this article, only the azimuth pattern characteristics while scanning gets maximum focus. The amplitude values are realized by a symmetric power divider with a unit input power, and all elements have equal phase feeding.
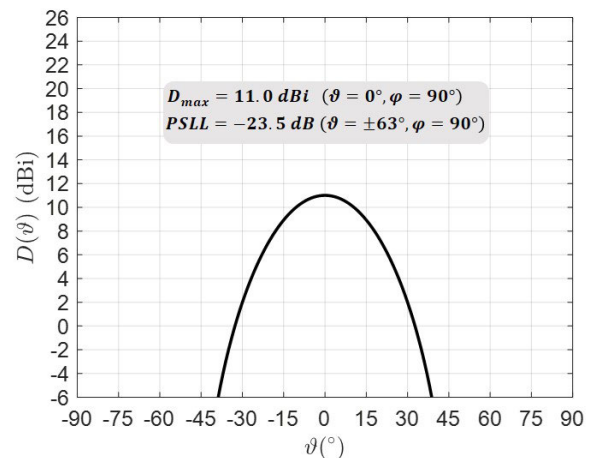
The scanned subarray pattern for $\varphi = 90°$ is plotted in Fig. 12, while the pattern $\varphi = 0°$ is just a cosine theta function. It is obvious that this subarray is not ϑ_0 dependent as it is oriented along the y'-axis. The maximum directive gain is $D_{max} = 11.0$ dBi, while the PSLL (at $\varphi = 90°$) is 23.5 dB below the mainlobe level. It can be analyzed that, with two extra elements without additional T/R modules, on the top and bottom sides of the linear array along the x-axis, the directive gain is increased significantly. In addition, the sidelobe in the elevation pattern can be substantially suppressed. The elevation ($\varphi = 90°$) beamwidth of 36° is suitable for surveillance applications, with azimuth scanning in both negative and positive ϑ angles. It is noted that the cross-line subarray pattern in the azimuth plane ($\varphi = 0°$) is just a $cos(\vartheta)$-pattern, meaning that this subarray is primarily used for adjusting the elevation pattern around $\varphi = 90°$.

The second configuration, Type 3b, with $B_{p3,n}^{(3)} = [0.23; 0.95; 0.23]$ is also examined. The amplitudes are chosen by considering a lower total amplitude values compared with the first configuration, Type 3a, to obtain a lower step for realizing a reference amplitude distribution.

The scanned subarray pattern for $\varphi = 90°$ is plotted in Fig. 13, whereas the pattern at $\varphi = 0°$ is the cosine theta function. Also, here the pattern is not ϑ_0 dependent. As expected, a lower directive gain, $D_{max} = 9.7$ dBi, is obtained, compared with subarray Type 3a. Meanwhile, there is no SLL in both azimuth and elevation patterns. The elevation ($\varphi = 90°$) beamwidth of 48° is wider than subarray Type 3a, but still acceptable for surveillance applications, with only scanning in both negative and positive ϑ angles. The pattern in the azimuth plane ($\varphi = 0°$), is again just a $cos(\vartheta)$-pattern.

These subarrays do not affect the sidelobes of the full array in the azimuth plane because the subarray elements are located along the y-axis. In the elevation plane, these subarrays help to narrow the elevation beamwidth.
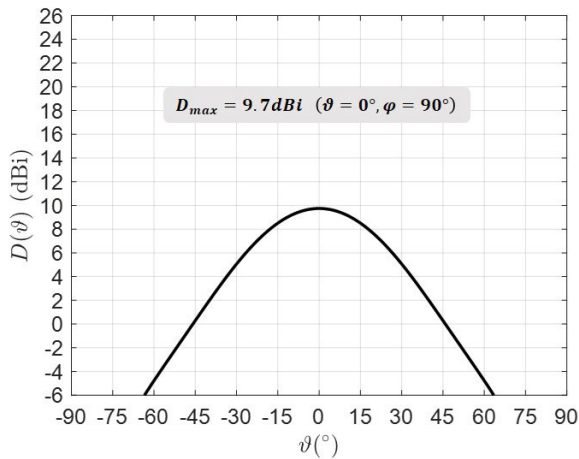
FIGURE 13. Elevation pattern ($\varphi = 90°$) of the subarray Type 3b (3 elements parallel to y-axis), with $B_{P3b,n}^{(3b)} = [0.23; 0.95; 0.23]$ and $\lambda/2$-grid elements. This subarray pattern is not ϑ_0 dependent.

TABLE 2. Location of the element of the subarray Type 4a in the left half side of the configuration.

Element number ($p_{4a,n}$)	Location ($x'p_{4a,n}$) in λ	Spacing to next element in λ	Associated amplitude	Reference Taylor amplitude
1	-2.95	0.53	0.88	0.88
2	-2.42	0.51	0.92	0.91
3	-1.91	0.49	0.96	0.95
4	-1.42	0.48	0.98	0.97
5	-0.94	0.47	1	0.98
6	-0.47	0.47	1	0.99
7	0	-	1	1

D. SUBARRAY TYPE 4

1) SUBARRAY TYPE 4a

In this subarray, an arbitrary $P_{4a,n}$ number of elements can be used. For the final array discussed in Section IV, this subarray has $P_{4a,n} = 13$ elements, and therefore, the center element is at subarray element number 7. The maximum spacing equals 0.53λ for avoiding grating lobe effects at a maximum scan angle $\vartheta_{0\_max} = 60°$. The virtual amplitudes are determined by positioning the elements at the locations for matching the amplitudes with the wanted amplitude Taylor distribution. We use herein the Taylor amplitude distribution for achieving -30 dB SLL.

The element located in the left half of the subarray configuration is presented in Table 2. It can be seen that the element locations are stretched with spacing values from 0.47λ up to 0.53λ. The minimum spacing depends on the actual antenna physical size as used in the full array of Section IV, which in our case, is 0.47λ. For elements number eight up to 13, the spacing values are just the mirror of these values. These spacing values are a substitution of the Taylor tapered amplitude values, where the minimum spacing determines the highest value over the array, i.e. 1. The transformation of the amplitude distribution into the spacing is performed following the procedure elaborated in [14] but in a reverse way.
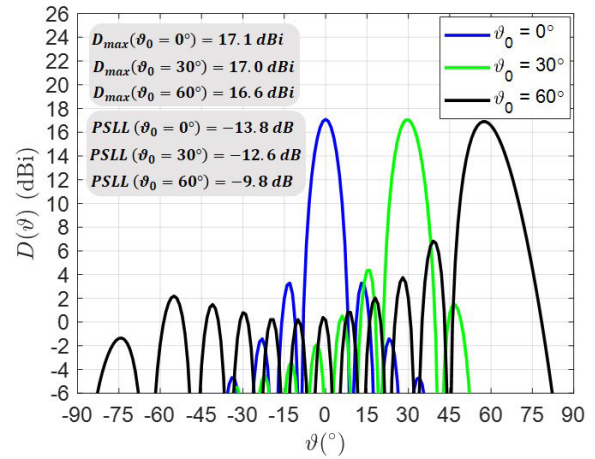

FIGURE 14. Scanned pattern ($\varphi = 0°$) of the subarray Type 4a with $P_{4a,n} = 13$ equal amplitudes, and various inter-element spacing stretched from 0.47λ up to 0.53λ. The patterns are obtained for positive scanning angles, $\vartheta_0 = 0°$, $30°$, and $60°$.

As shown in Table 2, the 6th and 7th elements use the minimum spacing value, 0.47λ. It means that 0.47λ corresponds to a relative amplitude of 1 for the 7th (center) element, while the spacing of the last elements corresponds to the ratio of $\frac{0.47\lambda}{0.53\lambda}$, which results in relative amplitude of 0.88 for the first (edge) element. This lowering amplitude is applied to achieve the maximum spatial stretching. Table 2 shows that the associated equivalent amplitude of each element matches with the reference Taylor amplitude, although in the application, all elements are given equal input power. The configuration of the last element should match the successive element in subarray Type 4b, which means that the successive element must have an associated virtual amplitude below 0.88.

The scanned subarray patterns are plotted in Fig. 14, where the phase shift factor of each element is obtained from the scan angle and the element location in the array configuration. For broadside scanning, the maximum directive gain, D_{max}, of 14.1 dBi is obtained, while the PSLL is 13.8 dB below the mainlobe level. It has been analyzed that a maximum directive gain is obtained due to the use of uniform amplitude distribution, and a slightly lower PSLL is realized compared with a Uniform Linear Array (ULA). For 30° scanning, the maximum directive gain, D_{max}, of 14.0 dBi and the PSLL of 12.6 dB below the mainlobe level are obtained. The scanned mainlobe level is not much changed, only 0.1 dB lower, compared with scanning at broadside direction, while the PSLL is increased due to the scanned array. For 60° scanning, the maximum directive gain, D_{max}, of 13.6 dBi and a PSLL of 9.8 dB below the mainlobe level are achieved. The mainlobe level gets -0.5 dB scan-loss only; the limited scan-loss in this dense linear array with stretching comes from the lowering in radiated power as a function of scan angle. The obtained high sidelobe is a grating lobe effect due to the scanning to a large scan angle of $-60°$. In the construction of the full array pattern, this subarray is only for lowering the sidelobes, particularly the near sidelobe due to spatial stretching, and no effect on the scan loss compensation.
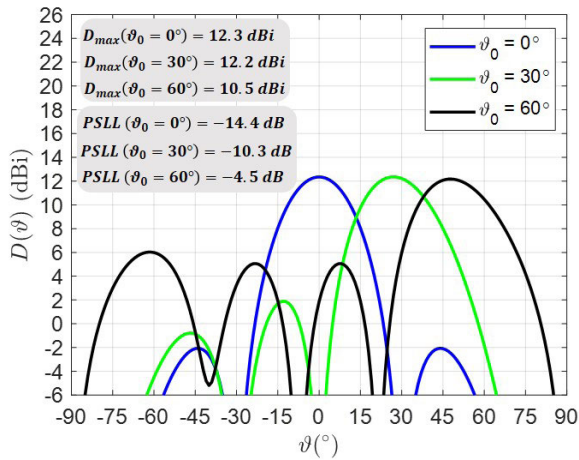
FIGURE 15. Scanned pattern ($\varphi = 0°$) of the subarray Type 4b with $P_{4b,n} = 4$ equal amplitudes, and various inter-element spacing stretched from 0.47λ up to 0.53λ. The patterns are obtained for positive scanning angles, $\vartheta_0 = 0°$, $30°$, and $60°$.

2) SUBARRAY TYPE 4b

This subarray uses a smaller number of elements than the previous configuration, subarray Type 4a. The number of elements $P_{4b,n} = 4$ is selected in this design for either the left or right side. It means that there are two subarrays Type 4b, with a total of eight elements, in the full array to fill in the left and right sides. In this subsection, only the 4b-Type subarray on the left side of the Type 4a is discussed. Following similar considerations, as for subarray Type 4a the maximum spacing is 0.53λ, while the minimum spacing is 0.47λ.

The element locations of this configuration are shown in Table 3, and also the associated amplitude distribution corresponding to the spatial stretching. These spacing values are the substitution of the relative amplitude value, where the minimum spacing determines the maximum relative value over the four elements array, i.e. 1. In the application, this maximum value, determined by element 4, is related to the minimum value or the last edge element in the subarray Type 4a. The minimum tapering value obtained in subarray Type 4a is 0.88; it means that element 4 must have a tapering value below 0.88. In our design we select an amplitude of 0.87, due to the use of a large spacing between element 4 of subarray 4b and the last element of subarray 4a. Then the last element (element 1) has an associated amplitude of 0.74 corresponding to the spacing of 0.53λ. The associated amplitude distribution obtained from the spatial stretching also approximates well the reference Taylor distribution as shown in Table 3. By matching the Taylor distribution with the associated amplitude, especially in the transition between subarrays Type 4a and 4b, the optimum spacing between the last edge element of subarray Type 4a and the edge element of subarray Type 4b has been obtained to be 0.56λ. As a result, the approximation of the entire Taylor amplitude distribution is accomplished only with spatial stretching and uniformly fed elements.

TABLE 3. Locations of the elements of subarray Type 4b in the left side configuration.

Element number $(p_{4b,n})$	Location $(x'_{p_{4b,n}})$ in λ	Spacing to next element in λ	Associated amplitude	Reference Taylor amplitude
1	-1.49	0.53	0.74	0.74
2	-0.96	0.49	0.80	0.79
3	-0.47	0.47	0.84	0.84
4	0	0.56*	0.88	0.88

*Spacing to the edge element of subarray Type 4a

The scanned patterns of this subarray is plotted in Fig. 15, where the phase shift factor of each element is derived from the scan angle and the 'real' element location in the full array configuration. For broadside scanning, the maximum directive gain, D_{max}, of 9.3 dBi is obtained, while the PSLL is 14.4 dB below the mainlobe level. The maximum directive gain is achieved due to the uniform amplitude distribution, and the pattern produces a slightly lower PSLL compared with a ULA. For 30° scanning, the maximum directive gain, D_{max}, of 9.2 dBi and the PSLL of 10.3 dB below the mainlobe level are obtained. The scanned main lobe level is changing, only -0.1 dB lower, compared with broadside direction, while the PSLL is increased due to the scanning. For 60° scanning, the maximum directive gain, D_{max}, of 7.5 dBi and a PSLL of 4.5 dB below the mainlobe level are obtained. The mainlobe level exhibits -1.8 dB scan-loss only because the radiated power dependence on the scan angle has been taken into account in the directive gain calculation. The obtained high PSLL is a grating lobe due to scanning to a large scan angle, 60°. This subarray has the same effect on the full array pattern construction as subarray Type 4a, which can lower the near sidelobe due to the spatial stretching located next to subarray Type 4a. In general, the scan loss is still not compensated in this linear array without the presence of subarrays Type 1 and Type 2.

3) SUBARRAY TYPE 4c

In this design, the number of elements, $P_{4c,n} = 3$, is only 3, and only subarray located at the left edge side is discussed here. The amplitude values are determined by fitting the amplitudes with the desired Taylor amplitude tapering distribution at the same location. In this article, the amplitude values of $B_{n^{(4c)}} = [0.9; 0.95; 1]$ are used because a flat edge amplitude taper over linear arrays leads to low PSLL in the broadside pattern. The subarray patterns are plotted in Fig. 16, where the phase shift factor of each element is obtained from the scan angle and the 'real' element location in the full array configuration. For broadside scanning, the D_{max} of 8.2 dBi and a PSLL of 17.2 dB below the mainlobe level are obtained. It can be analyzed that a low PSLL compared to that of a ULA is obtained due to the use of tapered amplitudes. For 30° scanning, $D_{max} = 8.0$ dBi and PSLL is 9.5 dB below the mainlobe level. As discussed before, the scanned directivity level is changing only 0.1 dB lower, while the PSLL is increased with scanning. For 60° scanning, $D_{max} = 5.7$ dBi
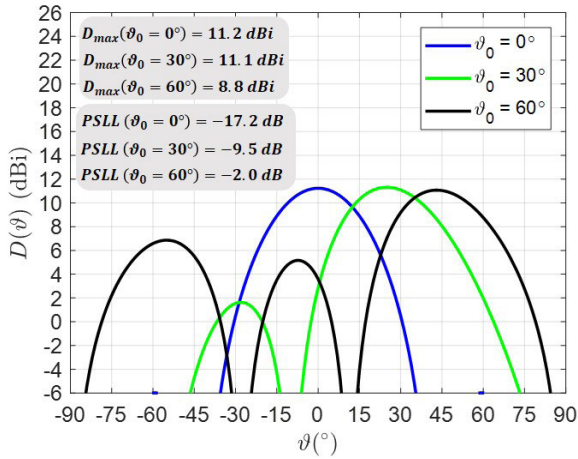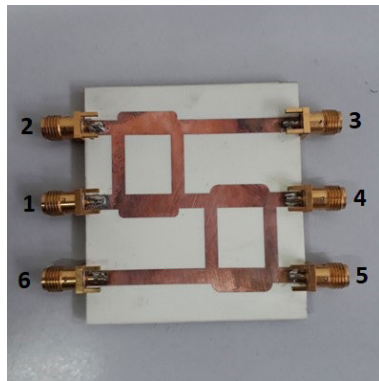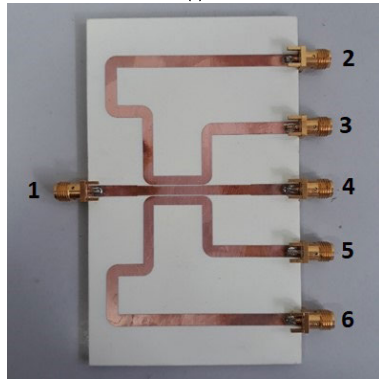
FIGURE 16. Scanned pattern ($\varphi = 0°$) of the subarray Type 4c with $P_{4c,n} = 3$, $\lambda/2$-grid elements and amplitude of $B_{n(4c)} = [0.9; 0.95; 1]$ for $p_{4c,n} = 1, 2,$ and 3. The patterns are obtained for positive scanning angles, $\vartheta_0 = 0°, 30°,$ and $60°$.

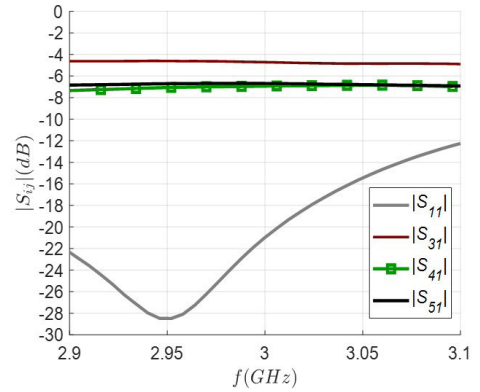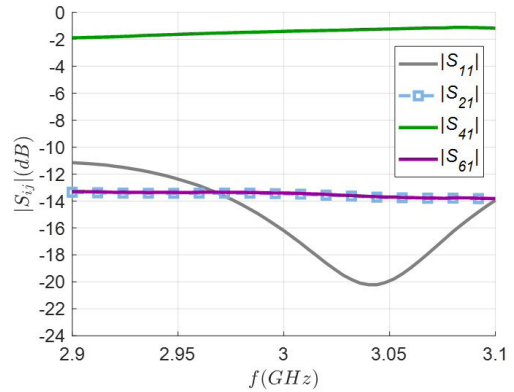FIGURE 17. Realization of the power dividers for two subarray designs. (a) Type 3a; (b) Type 3b.

FIGURE 18. The measured S-parameters results of the power divider designs in Fig. 17 Note that the correct phase values are realized by adding coaxial cable extension with a certain length. (a) Subarray Type 3a; (b) Subarray Type 3b.

E. REALIZATION AND EXPERIMENTAL VALIDATION OF SUBARRAY TYPES 3a AND 3b

In this subsection, the subarray Type 3 is realized using CUP antennas as elements and fed with microstrip-based power dividers to produce the desired amplitude distribution. The realized subarrays operate at a center frequency of 3 GHz. There are two designs that are realized

1) Subarray Type 3a with amplitude distribution of $B_{p3a,n}^{(3a)} = [0.505; 0.7; 0.505]$; the sum of the amplitudes equals 1.71.
2) Subarray Type 3b with amplitude distribution of $B_{p3b,n}^{(3b)} = [0.23; 0.95; 0.23]$; the sum of the amplitudes equals 1.41.

The realization of the power dividers for the subarrays Type 3a and 3b are shown in Fig. 17a and Fig. 17b, respectively. The power divider in Fig. 17a consists of two cascaded quadrature couplers with port 1 as an input port, ports 3, 4, and 5 as output ports producing power of 0.49, 0.255, and 0.255, respectively; port 3 feeds the center element, while port 4 and 5 feed the upper and lower elements, respectively. Ports 2 and 6 are isolated ports and loaded with 50Ω terminations. Power divider in Fig. 17b is based on coupled line couplers with port 1 as input port and ports 2, 4, 6 as output ports producing

and PSLL is 1.9 dB below the mainlobe. The mainlobe level undergoes a -2.5 dB scan-loss due to the $cos(\vartheta)$-pattern, while the PSLL is higher than in the previous configuration. This large scan-loss occurs due to the fact that only three elements are used in this subarray. The contribution of this subarray is mostly the same with two previous subarrays, namely Type 4a and 4b, but this subarray uses amplitude control to obtain lower amplitude level for SLL suppression in the full array.
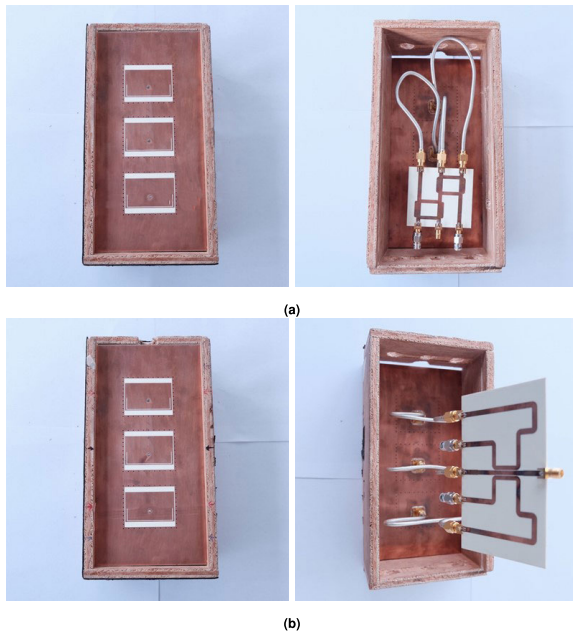
FIGURE 19. Fabricated modular cross-line subarrays: (a) Front (left) and back (right) view of the subarray Type 3a; (b) Front (left) and back (right) view of the subarray Type 3b.

powers of [0.05, 0.9, 0.05] by adjusting the spacing between the lines. For each power divider, the output power summation provides a unit power at the subarray input ports. Besides that, ports 3 and 5 are isolated and loaded with $50\,\Omega$ terminations.

The measured S-parameters of both couplers are presented in Fig. 18. It can be seen that the measured return losses $|S_{11}|$ for both couplers are below $-15\,$dB at the operational frequency of $3\,$GHz. The measured coupling losses of the power divider for the Type 3a realization (presented in Fig. 17a), $|S_{31}|$, $|S_{41}|$ and $|S_{51}|$, are flat around $-4.7\,$dB, $-6.9\,$dB, and $-6.7\,$dB, respectively. For the Type 3b design (presented in Fig. 17b) the values of $|S_{21}|$, $|S_{41}|$ and $|S_{61}|$ are around $-13.4\,$dB, $-1.4\,$dB, and $-13.4\,$dB, respectively. For the phase measurement, additional coaxial cables are added to produce the same phase at all output ports.

The realizations of subarrays Type 3a and Type 3b are displayed in Fig. 19a, and Fig. 19b, respectively. The power divider network is located behind the antennas and connected via coaxial cables. The simulated patterns and measurement results, at 3 GHz, of the fabricated subarrays, are shown in Fig. 20. The magnitude pattern of the subarray Type 3a shown in Fig. 20a indicates that the elevation pattern has $-20\,$dB SLL and narrower beam than the azimuth pattern, whereas the magnitude patterns of the subarray Type 3b shown in Fig. 20b indicates that the elevation pattern also has a narrower beam than the azimuth pattern but not as much as in the Type 3a design. All measured data are compared with the patterns obtained from the theoretical calculation by using the exact equation shown in the previous section. The elevation patterns for both types are similar to the theoretical patterns. The deviation in amplitude is explained by
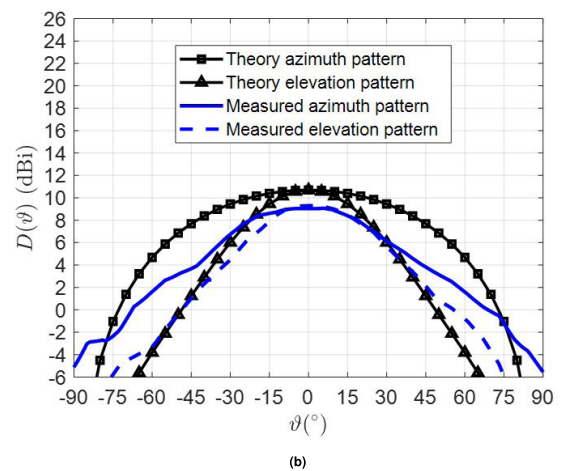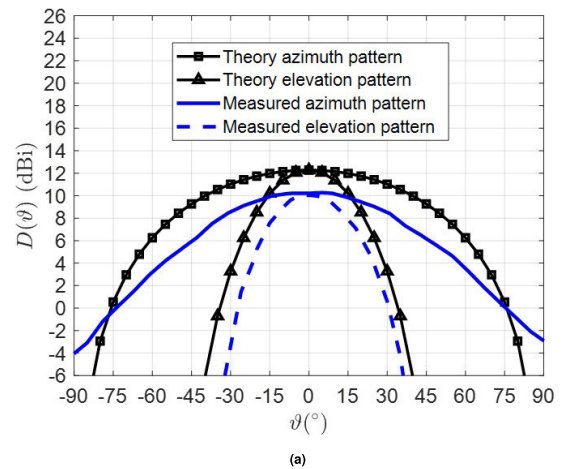

FIGURE 20. The magnitude pattern comparison between measurement and theoretical calculation results in azimuth and elevation plane. (a) Subarray Type 3a; (b) Subarray Type 3b.

limitations in the measurement set up, taking into consideration the low directive gain of the subarray, the subarray's small ground plane relative to the wavelength, the difficulty of absolute gain calibration of low gain antennas and antenna measurement accuracies in the anechoic chamber.

In the case of the azimuth pattern, the measured results for both types are slightly wider than the theoretical pattern; the measured pattern loss at $60°$ is just 1 dB lower than the theoretical pattern. The elevation and azimuth phase patterns for both subarrays are also measured, which are found to be flat around $\vartheta = 0°$. These measured outcomes of the subarrays indicate their reliability when integrated in a phased array.

IV. SUBARRAYS INTEGRATION FOR CONSTRUCTING THE FULL PLANAR ARRAY
A. STEP-BY-STEP INTEGRATION
In the previous section, all subarrays in the toolbox have been individually designed and optimized. In this section, all designed subarrays in the toolbox are integrated to form a full planar array with a maximum of 41 elements in length and a maximum of 3 elements in width. For deriving the amplitude
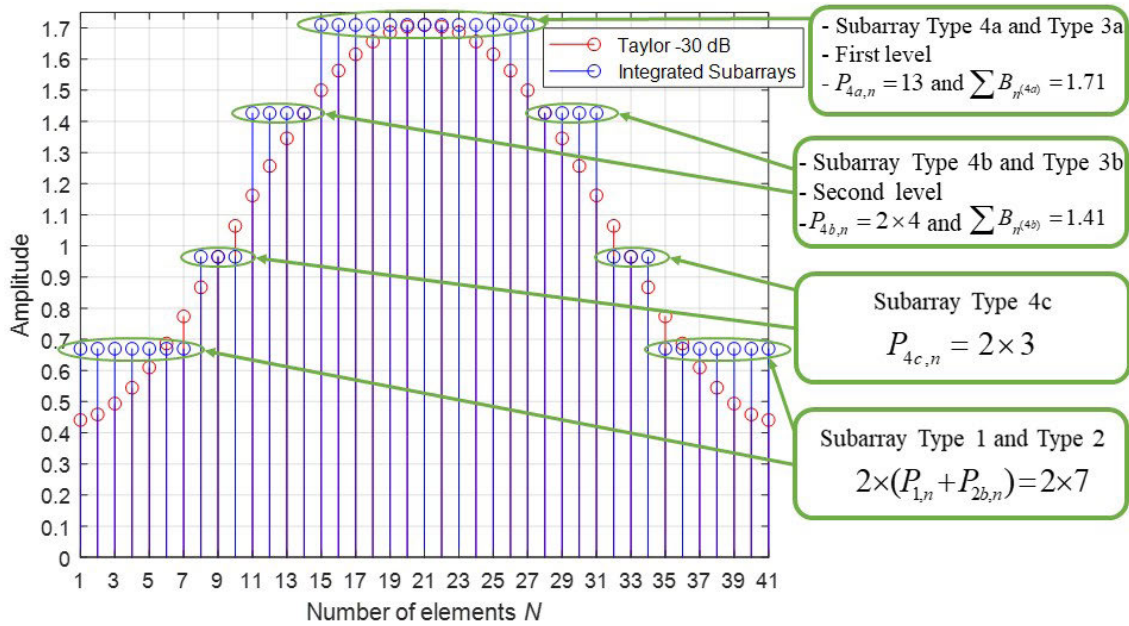
FIGURE 21. The amplitude divisions over the array of 41 elements.

tapering over the 41 elements, a linear array with a Taylor tapering and $-30\,\mathrm{dB}$ SLL is used in the start of the planar array design.

As explained in the previous section, the 3-element cross-line subarrays are used with equal input power, each divided over the three elements. Amplitude control is realized with a 1-to-3 power divider with a pre-defined division ratio. Normalization is done so that for an output power ratio of 0.25, 0.5, 0.25 the sum amplitude is maximum and equals $\sqrt{0.25} + \sqrt{0.25} + \sqrt{0.5} = 1.71$. It means that in the reference linear array, the Taylor distribution should also be normalized to a maximum amplitude of 1.71. In order to visualize the optimum fit with the Taylor amplitude distribution, the array division into subarrays is presented in Fig. 21. It can be seen that the array is divided into 4 levels starting from the center down to the edges. The first level to realize a uniform amplitude of 1.71 is around the center part where 13-element Subarray Type 4a in combination with cross-line Subarrays Type 3a are used. All Type 4a elements, or the cross-line Type 3a subarray feeds, use individual phase shifters only as indicated in Section II-D, for scanning to a certain direction. In addition, symmetric spatial stretching is also used to produce a 'virtual' tapering which follows the Taylor distribution.

The second level in the center part of the planar array represents the extension of the first level located in the left and right sides. It uses the spatially stretched 4 elements of in-line subarray Type 4b, at each side, in combination with the cross-line subarray Type 3b, to realize uniform amplitudes of 1.41. All elements of Type 4b subarray (or the feeds of the cross-line Type 3b subarrays) use individual phase shifter as indicated in Section II-D, for scanning to a certain

direction. This second level of 1.41 can realize the requred 'virtual' tapering by stretching, which otherwise cannot be realized by stretching the elements using only the first level of 1.71 over the whole center part, without exceeding the maximum allowed spacing requirement. The spacing between the in-line subarrays is calculated based on the reference Taylor amplitude at the same location.

The next level in the center part is for matching the tapering distribution between the center part and the edge parts. This level uses 3-element subarray Type 4c, at each side, where amplitude control is used to realize tapering values below the amplitude level of 1. The use of attenuators can be substituted with spatial stretching in case the tapering values are lower than the maximum allowed spacing. All subarray 4c elements use individual phase shifters, as indicated in Section II-D, for scanning to a certain azimuth direction. In addition, the spacing between this subarray and the one in the second level is also calculated by considering the reference Taylor amplitude at the same location. With the use of subarrays 3a, 3b, 4a, 4b, and 4c, the center part of the array has been built up.

The edge parts of the planar array consist of subarrays for compensating the scan-loss, i.e. those of Types 1 and 2. The optimum configuration in this part is referring to the configuration in [40], where the 2 elements subarray along the *x*-axis is located next to the matching layer, while the two 3 elements subarrays with one element in overlap (i.e., the 5 elements Type 2b) are located next to it. The individual subarrays with 3 elements have one input at the subarray center and have normalized input power. The location of the inputs determines the location of the 3 elements subarrays in the full array.

Following the design strategy, each part is integrated step by step from the center to the edges for analyzing the integration effect to the full array performance. The array performance analysis is conducted for the scanning array and results into the azimuth patterns for azimuth scan angles of broadside, 30°, and 60° scanning and the elevation pattern for broadside scanning.

STEP 1: INTEGRATE SUBARRAYS TYPE 3a INTO THE SUBARRAY TYPE 4a (THE FIRST LEVEL OF CENTER PART)

The first step is integrating the in-line subarray Type 4a with stretching along the x-axis and cross-line subarray Type 3a with a fixed $\lambda/2$-grid. It means that all elements of the subarray Type 4a become the center elements of subarray Type 3a. The number of elements used in subarray Type 4a is 13, which are fed with equal amplitudes of 1.71, for which the spacing is stretched with a minimum of 0.47λ in the middle up to 0.5359λ in the edges. For the azimuth pattern and element spacing of 0.47λ the maximum amplitude in the $\varphi = 0°$ projection plane becomes 1.71, while for the spacing of 0.5359λ the amplitude is 0.877 times 1.71. Subarray Type 3 has $\lambda/2$-grid elements and located perpendicular to the array x-axis and uses unequal amplitudes to produce a lower SLL in the elevation pattern. The amplitude values are then $B_{p_{3a,n}}^{(3a)} = [0.505; 0.7; 0.505]$ for $p_{3a,n} = 1, 2,$ and 3. This amplitude distribution is realized by using an equal-phase power divider without attenuators. It means that the maximum amplitude value obtained by this subarray is 1.71, which is represented by the spacing of 0.47λ, while the minimum amplitude is 1.5, represented by the spacing of 0.5359λ.

The full array patterns, in azimuth and elevation, of this configuration are shown in Fig. 22. It can be seen from the azimuth pattern in Fig. 22a that the maximum directive gain is high due to the gain of subarray Type 3b, particularly at broadside direction. Meanwhile, for scanning to $\vartheta_0 = 60°$, it goes down significantly following the shape of the element pattern. The PSLL of this configuration is located in the first side lobe (FSLL), which goes up when the antenna is scanned to $\vartheta_0 = 60°$. A further SLL suppression is needed for improving this array performance. The elevation pattern shown in Fig. 22b indicates that the narrower elevation pattern is obtained, due to the use of subarray Type 3b. The array performance of the two Types of 3a and 4a subarrays is summarized in Table 4, shown later in this section.

STEP 2: INTEGRATE SUBARRAYS TYPE 3b IN THE SUBARRAY TYPE 4b (THE SECOND LEVEL OF CENTER PART)

In the second level on the left and right sides of the center part, subarray Type 4b is integrated with subarrays Type 3b. It means that all elements of the in-line subarray Type 4b are substituted with cross-line subarray Type 3b, which have amplitude of $B_{p_{3b,n}}^{(3b)} = [0.23; 0.95; 0.23]$ for $p_{3b,n} = 1, 2,$ and 3. All elements of the subarray Type 3b are located at a $\lambda/2$-grid perpendicular to the array x-axis. Subarray Type 4b uses 4 elements at each left and right sides, and therefore the total number of elements in the full array is then 21
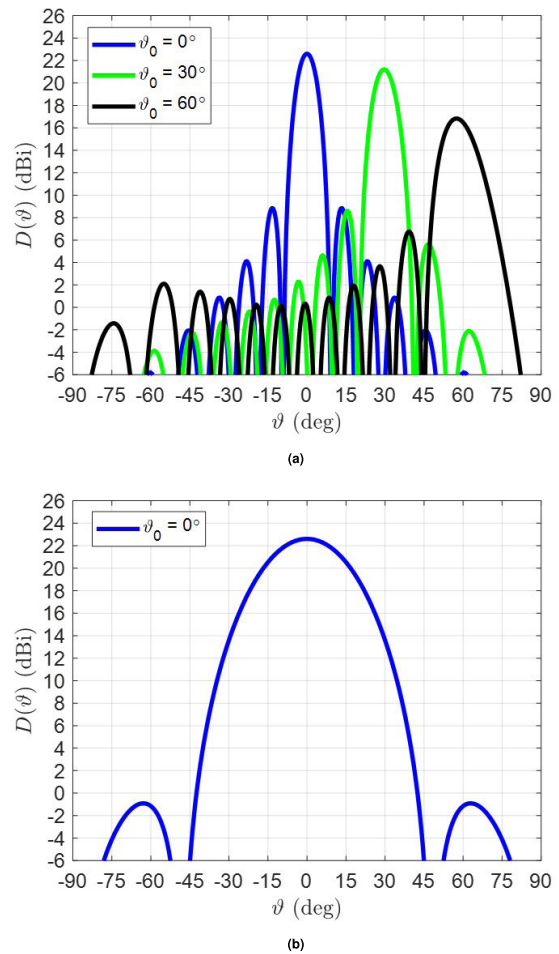

FIGURE 22. Array patterns of the subarray Type 4a ($P_{4a,n} = 13$, uniform amplitudes, and stretched spacing) integrated with subarray Type 3a with amplitude distribution of $B_{p_{3a,n}}^{(3a)} = [0.505; 0.7; 0.505]$ for $p_{3a,n} = 1, 2,$ and 3. (a) azimuth pattern while scanning from broadside up to $\vartheta_0 = 60°$; (b) elevation pattern for broadside scanning.

elements. The inter-element spacing of these 4 elements are also stretched, to follow a Taylor tapering, with a minimum spacing of 0.47λ up to a maximum of 0.5359λ. The minimum spacing is used by the element located next to the last element of the first level, which is equivalent to an amplitude of 1.41. Meanwhile, the maximum spacing is used by the last edge element, which results in an amplitude of 1.24. This configuration is applied for both sides.

The array patterns of the configuration after steps 1 and 2 are presented in Fig. 23 It is noted for the azimuth pattern (see Fig. 23a) that the maximum directive gain, obtained at broadside scanning, is higher than the previous result due to the use of extra elements at the edges. However, it still goes down significantly when the antenna is scanned to $\vartheta_0 = 60°$, which means that there is still no compensation in the scanloss. It should also be noted that, the SLLs are lower than the previous result because of the spatial stretching in the second level. In the elevation pattern, Fig. 23b, it can be observed that the HPBW at broadside scanning is also narrower than
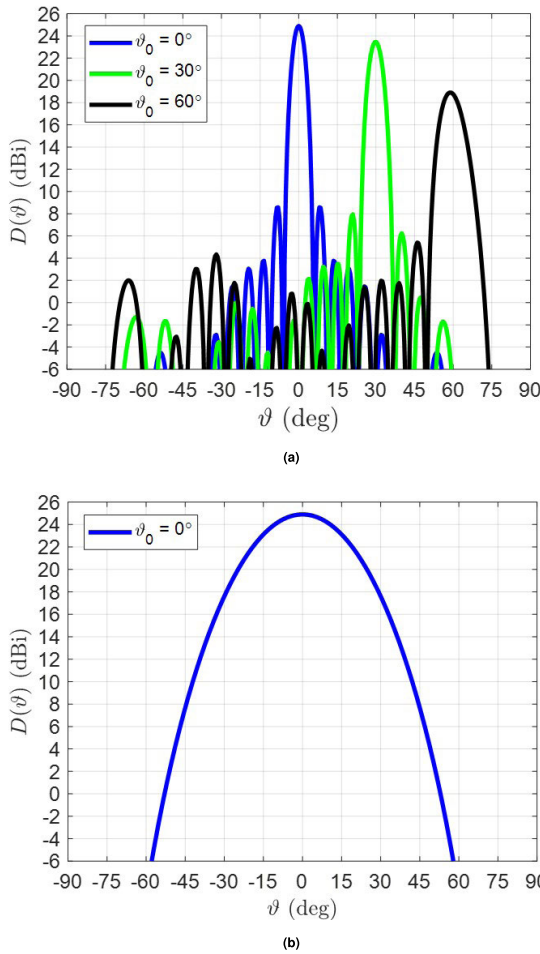
(a)

(b)

FIGURE 23. Array pattern of the subarray Type 4a ($P_{4a,n} = 13$, uniform amplitude, and stretched spacing) in combination with subarrayd Type 3a and 3b and subarray Type 4b ($P_{4b,n} = 2 \times 4$ for both sides, uniform amplitude, and stretched spacing). The power division in subarray Type 3b has an amplitude distribution of $B_{P3b,n}^{(3b)} = [0.23; 0.95; 0.23]$ for $p_{3b,n} = 1, 2,$ and 3. (a) azimuth pattern while scanning from broadside up to $\vartheta_0 = 60°$; (b) elevation pattern for broadside scanning.
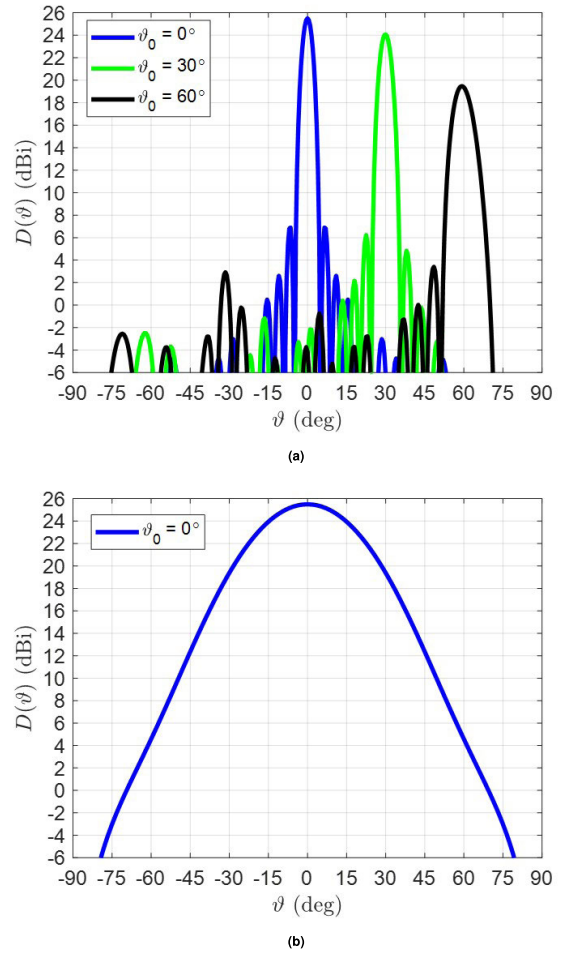

(a)

(b)

FIGURE 24. Array pattern of the subarray Type 4a ($P_{4a,n} = 13$, uniform amplitude, and stretched spacing) in combination with subarrays Type 3a and 3b and subarray Type 4b ($P_{4b,n} = 2 \times 4$ for both sides, uniform amplitude, and stretched spacing) in combination with subarray Type 3b, and matching layer ($P_{4c,n} = 2 \times 3$ for both sides). The amplitude of the elements in the left side matching layer (subarray Type 4c) is $B_n^{(4c)} = [0.9; 0.95; 1]$. (a) azimuth pattern while scanning from broadside up to $\vartheta_0 = 60°$; (b) elevation pattern for broadside scanning.

before due to the larger array dimension after the addition of subarrays Type 3b.

STEP 3: INTEGRATE SUBARRAYS TYPE 4c

After the first and second levels are integrated, the last subarray of the center part, namely the matching subarray Type 4c, is integrated in both left and right sides. This subarray is used for lowering the tapering and as the matching layer between the center part and the edge parts. There are 3 elements, located along the major array axis, with non-uniform amplitudes. The amplitude values, for the left side subarray, are $B_{n^{(4c)}} = [0.9; 0.95; 1]$. This amplitude distribution is selected to maintain slope similarity with the Taylor tapering. Because one subarray element has an amplitude 1 there are only 2 attenuators per subarray needed at each side. For the right side, the amplitude values are just the mirror of it.

After integration of steps 1, 2, and 3, the azimuth patterns, in Fig. 24a depict that the SLL is lower than the previous

configuration due to the use of the matching layer. However, the maximum directive gain while scanning to a large scan angle is still going down due to the element pattern, which means that there is still no scan loss compensation.

STEP 4: INTEGRATE SUBARRAYS TYPE 1 AT THE INNER PART OF THE EDGES

In the previous steps, subarray integration has been focused on increasing of the maximum directive gain and also lowering the SLL. In this step, the integration of subarrays Type 1 is for compensating the scan-loss due to the element pattern. This subarray is located at the edge part of the array configuration next to the matching layer. Subarray Type 1 uses amplitude of $B_{p1,n}^{(1)} = [0.7; 0.7]$ for $p_{1,n} = 1$ and 2, realized by an equal-split power divider. For compensating the scan-loss when the array is scanned to positive angles, this subarray uses phase shift factors of $+70°$ and $-70°$ for the left and right sides elements. When the array is scanned to negative

(a)

(b)

FIGURE 25. Array pattern of the subarray Type 4a ($P_{4a,n} = 13$, uniform amplitude, and stretched spacing) in combination with subarrays Type 3a and 3b and subarray Type 4b ($P_{4b,n} = 2 \times 4$ for both sides, uniform amplitude, and stretched spacing) in combination with subarray Type 3b, and matching layer ($P_{4c,n} = 2 \times 3$ for both sides), and subarray Type 1 with amplitude of $B_{P_{1,n}}^{(1)} = [0.7; 0.7]$ and phase shift factor of $\psi_{1_{1,n}} = [+70°; -70°]$ for $p_{1,n} = 1$ and 2. This phase shift factor value is used for positive scanning application. (a) azimuth pattern while scanning from broadside up to $\vartheta_0 = 60°$; (b) elevation pattern for broadside scanning.
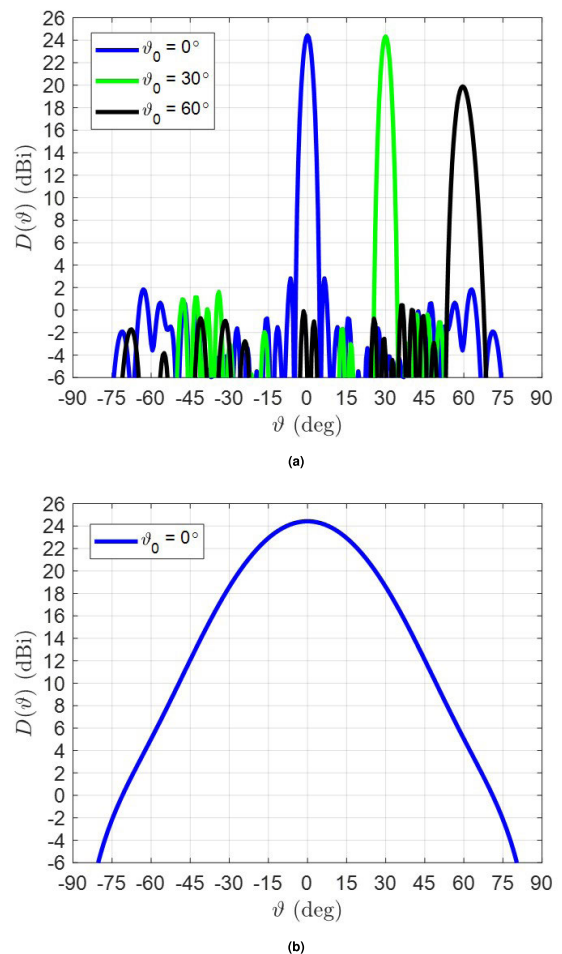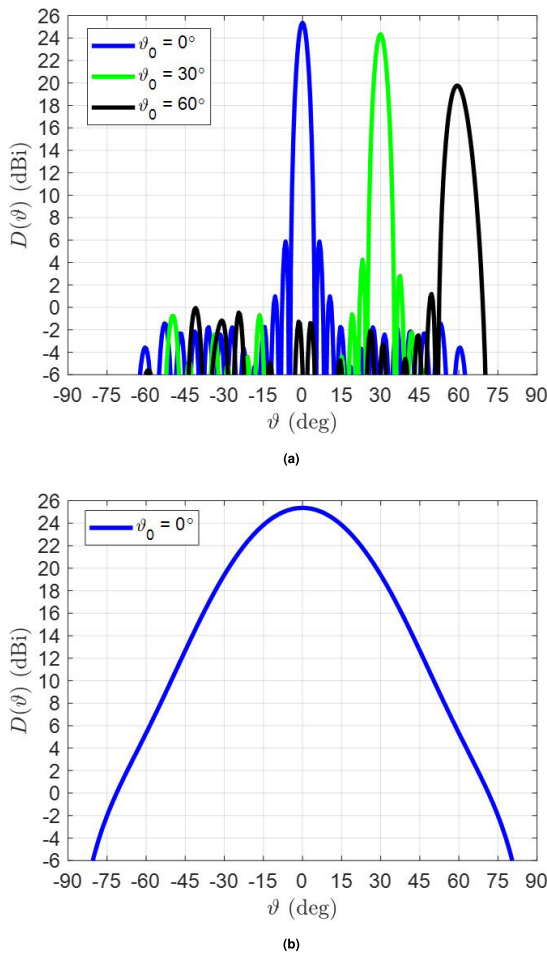

(a)

(b)

FIGURE 26. Array pattern of the subarray Type 4a ($P_{4a,n} = 13$, uniform amplitude, and stretched spacing) in combination with subarrays Type 3a and 3b and subarray Type 4b ($P_{4b,n} = 2 \times 4$ for both sides, uniform amplitude, and stretched spacing) in combination with subarray Type 3b, and matching layer ($P_{4c,n} = 2 \times 3$ for both sides), and subarray Type 1, and subarray Type 2b. The subarray Type 2b is constructed from two overlapped subarrays Type 2a with amplitude of $B_{P_{2a,n}}^{(2a)} = [0.41; 0.82; 0.41]$ and phase shift factor of $\psi_{P_{2a,n}}^{(2a)} = [+140°; 0; -140°]$ for $p_{2a,n} = 1$, 2, and 3. This phase shift factor value is used for positive scanning application. (a) azimuth pattern while scanning from broadside up to $\vartheta_0 = 60°$; (b) elevation pattern for broadside scanning.

angles, these values become the opposite and are realized by using 1-bit phase shifters.

After integration of steps 1 to 4, the azimuth pattern of the full array at this stage, as given in Fig. 25a, shows that the integration slightly affects the maximum directive gain while scanning to $\vartheta_0 = 60°$. It increases and, as a consequence, the scan-loss is lower. In addition, the SLLs are much lower than the previous configuration. It means that this subarray integration is not only for increasing the SLC, but can also lower the SLL while scanning. The elevation pattern, in Fig. 25b, is not much affected.

STEP 5: INTEGRATE SUBARRAYS TYPE 2b AT THE OUTER PART OF THE EDGES

The complete configuration by integrating the Type 2b subarrays are shown now. The subarrays Type 2b are integrated

in the outer part of the edge of the full array configuration. Like Type 1 subarrays, Type 2b subarrays are designed for compensating the scan loss due to the element pattern. A Type 2b subarray is constructed from two overlapped subarrays Type 2a, where the right side element of the first subarray coincides with the left side element of the second subarray. These overlapped elements are fed from the left and right sides. The subarray Type 2a in this configuration uses amplitude of $B_{P_{2a,n}}^{(2a)} = [0.41; 0.82; 0.41]$ for $p_{2a,n} = 1$, 2, and 3, and phase shift factor for the left and right sides elements are $+140°$ and $-140°$, respectively. These phase shift values are used when the array is scanned to positive angles. When the array is scanned to negative angles, the phase shift values become the opposite, with help from 1-bit phase shifters.
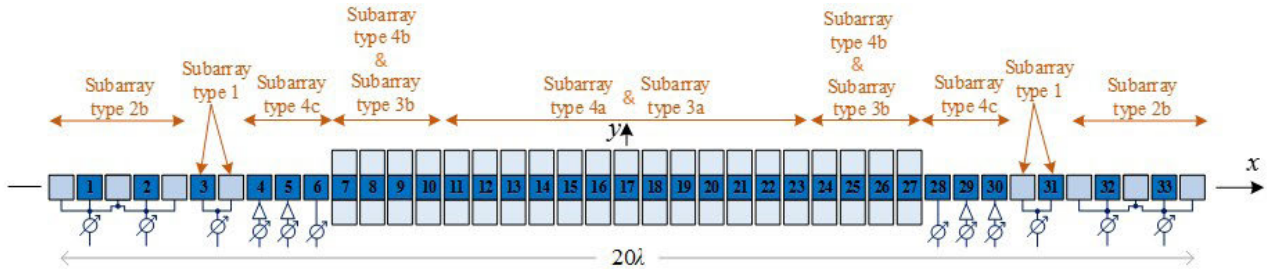
FIGURE 27. Final array configuration with all integrated subarrays. This diagram provides an example of the general case given in Fig. 1.

TABLE 4. Summary of the array pattern performances for each integration step.

Step	Number of controls	Scanning ϑ_0	D_{max} (dBi)	Scan-loss (dB)	HPBW Az-plane	FSLL (dB)	PSLL (dB)
Step-1 Integration of Type 3a	13 K-bit phase shifters	0°	22.6	0.0	8.2°	-13.8	-13.8
		30°	21.2	-1.4	9.4°	-12.6	-12.6
		60°	16.8	-5.8	14.3°	-10.1	-10.1
Step-2 Integration of Type 3b	21 K-bit phase shifters	0°	24.9	0.0	5.1°	-16.3	-16.3
		30°	23.5	-1.4	5.9°	-15.5	-15.5
		60°	18.9	-6.0	9.6°	-13.5	-13.5
Step-3 Integration of Type 4c	27 K-bit phase shifters, 6 attenuators	0°	25.5	0.0	4.2°	-18.6	-18.6
		30°	24.1	-1.3	4.8°	-17.8	-17.8
		60°	19.5	-6.0	8.1°	-16.1	-16.1
Step-4 Integration of Type 1	29 K-bit phase shifters, 4 1-bit phase switches, 4 attenuators	0°	25.4	0.0	4.1°	-19.5	-19.5
		30°	24.3	-1.0	4.4°	-20.1	-20.1
		60°	19.8	-5.6	7.4°	-18.6	-18.6
Step-5 Integration of Type 2b (Final configuration using a -30dB Taylor taper along x-axis)	33 K-bit phase shifters, 12 1-bit phase switches, 4 attenuators	0°	24.4	0.0	3.9°	-21.6	-21.6
		30°	24.3	-0.1	39.1°	-27.3	-22.7
		60°	19.9	-4.5	5.9°	-37.7	-19.5
Taylor reference Array -30 dB, $N = 41$, perpendicular subarray	41 K-bit phase shifters, 41 attenuators	0°	23.4	0.0	3.5°	-24.3	-24.3
		30°	22.0	-1.4	4.1°	-23.5	-23.5
		60°	17.2	-6.2	6.9°	-21.2	-21.2

The full array pattern of this configuration are shown in Fig. 26. It can be seen that the azimuth pattern while scanning enjoys scan loss compensation. The maximum directive gain when scanning from broadside up to 30° experiences almost no degradation. Even for 60° scanning, the maximum directive gain exhibits lower loss than the previous configuration. This is because the integration of subarrays Type 2b in the left and right edges contributes significantly to the compensation of the scan loss. Moreover, the SLLs are still very low. The elevation pattern shown in Fig. 26b is slightly changes compared with the previous configuration.

B. FINAL ARRAY CONFIGURATION AND PERFORMANCES SUMMARY

The final array configuration after all subarrays in the toolbox have been optimized and integrated is shown in Fig. 27 The dark-blue elements represent the location of the elements with actual feeding in the full array, while the light-blue elements represent the elements that get feeding via the subarrays. All elements with actual feeding are located along the x-axis.

It can be observed from Fig. 27 that the integration of a mirroring pair of Type 1 subarrays and another mirroring pair

of Type 2 into the full array removes eight feeding ports from the initial 41-element linear array. As a consequence, the total number of fed elements in the full array is only 33 with 33 K-bit phase shifters, 12 1-bit phase switches, and only 4 fixed attenuators. The attenuators adjust amplitudes of elements 4, 5, 29, and 30 for realizing amplitude matching between the center and edge parts. In addition, 21 fixed power dividers feeding the 3-element subarrays perpendicular to the array axis are used in the center part to make it comparable with the proposed final array.

The summary of the array pattern for each integration step is presented in Table 4, which shows how different subarray types in the toolbox serve different purposes in improving the array performance. The number of element controls is also indicated in the table. The performance of the new array is compared with the Taylor reference array. This reference array has the same planar array configuration (including the perpendicular subarrays) and uses a -30 dB Taylor taper along the x-axis of a 41 elements linear array.

It can be seen that the scan-loss at $\vartheta_0 = 60°$ is -6.0 dB before subarrays for SLC are integrated, which follows $cos(\vartheta)$ pattern of the element (see Step 3 in Table 4). After

integrating subarrays Type 1 in the left and right sides, the scan-loss lowers to -5.6 dB (Step 4), which implies 0.4 dB SLC. The scan-loss goes further to only -4.5 dB when the subarrays Type 2b are integrated in the left and right sides (Step 5). When compared to the reference array, the obtained SLC is better by 1.7 dB.

The use of subarrays Type 3a and 3b contribute to superior FSLL and PSLL performances after all subarrays are integrated, where the PSLL while scanning to $\vartheta_0 = 60°$ is -19.5 dB. When compared to the reference array, this improved SLC and PSLL performance is very attractive because the new design only uses 4 attenuators in the planar array configuration, whereas the Taylor tapered linear array requires 41 attenuators, i.e., as many as the elements.

To further demonstrate the superiority of our results, [43] is selected to be a comparison in several aspects because it optimizes the use of subarrays in the planar array configuration. First of all, our design has capability to scan up to $\vartheta_0 = 60°$, while in [43] only up to $\vartheta_0 = 40°$. Therefore, the PSLL and scan-loss comparison are only conducted at $\vartheta_0 = 30°$. In addition, a design with 30% number of the phase shifter is considered because our design has a similar ratio. Our design gives PSLL and scan loss of -22.7 dB and -0.1 dB, at $\vartheta_0 = 30°$, respectively. Meanwhile, in [43], -13.8 dB and -2.2 dB of PSLL and scan loss are obtained, respectively. This indicates that our design is superior in terms of scan-angles direction, PSLL, and SLC compared with 'Case 1' design in [43].

To conclude this section, it should be stressed that the resulting configuration serves as an example on how to exploit the different subarrays in the toolbox in designing an array of desired characteristics. Given the dimension of the initial linear array, the toolbox offers various possibilities in the trade-off among multiple performance objectives that include directive gain, sidelobe level, scan loss, elevation beamwidth, and the number of feeds and controls. The elementary subarrays have been provided in the toolbox, whose directive gains are given in Section II, while the design method for each type of subarray is elaborated in Section III and the integration steps into the full array are detailed above.

V. CONCLUSION

A planar array with improved SLL and SLC performance constructed from the integration of both in-line and cross-line subarrays have been reported. The array design focuses on the trade-off optimization between SLL, SLC, reducing the number of element controls, as well as maximizing the use of phase-only elements for beam steering. The analysis of each subarray type has been discussed in detail. The construction of the planar array starts with the center part of the array by integrating subarrays Type 4a and 4b with subarrays Type 3a and 3b, respectively, and subarray Type 4c, in the center part. All subarrays Type 4 are spatially stretched for suppressing the SLL by following Taylor tapering distribution, while subarrays Type 3 are for increasing the directive gain by

limiting the elevation beamwidth. In the edges of the center part, subarrays with two elements (Type 1) and five elements (Type 2b) are integrated as the extensions. These subarrays help to lower the scan-loss in the maximum scan angle due to the element pattern effect.

The constructed array has 83 elements in total; 21 elements along the x-axis have 3 elements cross-line subarrays and 20 elements have not. A PSLL of -19.5 dB and a scan-loss of -4.5 dB are obtained when the array with CUP antenna as an element is scanned to a maximum scan angle of $\pm 60°$. This result becomes a reliable validation that a planar array constructed from different subarrays can have trade-off performances between SLL and scan loss, with a less number of element control.

APPENDIX

With respect to Fig. 1, the pattern of the l-th subarray with P_l elements and its center at (x_n, y_n) is given by the well-known expression [41],

$$E_{l,n}(\vartheta, \varphi, \vartheta_0, \varphi_0) = cos(\vartheta) \sum_{p_{l,n}=1}^{P_{l,n}} B_{p_{l,n}}^{(l)}$$
$$\times exp\left[j \left(\eta_{p_{l,n}}^{(l)}(\vartheta, \varphi) + \psi_{P_{l,n}}^{(l)}(\vartheta_0, \varphi_0) \right) \right] \quad \text{(A.1)}$$

with $\eta_{p_{l,n}}(\vartheta, \varphi) = \beta_0 \, sin(\vartheta)[x'_{p_{l,n}} cos(\varphi) + [y'_{p_{l,n}} sin(\varphi)]$, where $n > N - L$ for the subarrays and $n \leq N - L$ for the isolated elements, whereas $B_{p_{l,n}}^{(l)}$ is real and $\sum_{p_{l,n}=1}^{P_{l,n}} \left| B_{p_{l,n}}^{(l)} \right|^2 = 1$ for normalization of the power divider network used for feeding the subarrays, it denotes the amplitude of excitation of the p_l-th element of the l-th subarray, $\beta_0 = \frac{2\pi}{\lambda}$ (λ is the wavelength in free-space), $(x'_{p_{l,n}}, y'_{p_{l,n}})$ gives the location of the p_l-th subarray element in the x', y' coordinate system of the l-th subarray, and $\psi_{p_{l,n}}^{(l)}$ denotes the phase shift factor of the p_l-th subarray element in the l-th subarray. $\psi_{p_{l,n}}^{(l)}$ should be optimized for a certain scan angle (ϑ_0, φ_0) in order to allow for an improved SLC as will be demonstrated in the later sections.

Computing the directive gain of a radiating antenna array requires solving the integration of far-field radiating power density over a sphere. The analytical expression of the directive gain of a planar array with arbitrary element locations and amplitudes has been derived in [42]. A novelty in this article is the analytical expression that has been adjusted for directive gain computation of such planar arrays with integrated subarrays. For instance, the numerator of the directivity equation in [42] is re-written herein in more details as the sum of two series representing the isolated elements and the subarrays, respectively, whereas adjustments for the denominator are described below. It is noted that the integral equation determines the radiated power, depends on (ϑ_0, φ_0) and takes the mutual coupling between all (non-overlapped and overlapped) radiating elements into account. Taking all of these into consideration, the expression of the directive gain in [42] becomes as formulated in (A.2), as shown at the top

$$D(\vartheta_0, \varphi_0) = 2 \frac{\left| \sum_{n=1}^{N-L} A_n cos(\vartheta) exp[j(\xi_n(\vartheta, \varphi) + q_n(\vartheta_0, \varphi_0))] + \sum_{n=N-L+1}^{N} \sum_{l=1}^{L} A_n E_{l,n}(\vartheta, \varphi, \vartheta_0, \varphi_0) exp[j(\xi_l(\vartheta, \varphi) + q_l(\vartheta_0, \varphi_0))] \right|^2}{\sum_m^N \sum_n^N \sum_{p_{l,m}}^{P_{l,n}} \sum_{p_{l,n}}^{P_{l,n}} A_n A_m B_{p_{l,n}}^{(l)} B_{p_{l,m}}^{(l)} exp[j\Delta\psi + j\Delta q] 2^{0.5}\Gamma(1.5) \frac{J_{1.5}(Z_{m,n})}{Z_{m,n}^{1.5}}}.$$

$$(A.2)$$

of the next page, where $E_{l,n}(\vartheta, \varphi, \vartheta_0, \varphi_0)$ contains the phase factor $\psi_{p_{l,n}}^{(l)}$ of the subarrays for scan-loss compensation as given in (1), and

$$\xi_n(\vartheta, \varphi) = \beta_0 \, sin(\vartheta)\{x_n cos(\varphi) + y_n sin(\varphi)\};$$
$$q_n(\vartheta_0, \varphi_0) = -\beta_0 \, sin(\vartheta_0)\{x_n cos(\varphi_0) + y_n sin(\varphi_0)\};$$
$$\Delta\psi = \psi_{p_{l,n}}^{(l)} - \psi_{p_{l,m}}^{(l)};$$
$$\Delta q = q_n - q_m;$$
$$Z_{m,n} = \beta_0 \{(x_n - x_m + x'_{p_{l,n}} - x'_{p_{l,m}})^2$$
$$+ (y_n - y_m + y'_{p_{l,n}} - y'_{p_{l,m}})^2\}^{\frac{1}{2}}$$

The first series of the numerator on the right hand side of (A.2) refers to the array pattern that includes all isolated elements with $cos(\vartheta)$–pattern, where $1 \leq n \leq N - L$. A_n and q_n denote the amplitude and the phase shift factor of the n-th isolated element in the array, respectively, the latter being dependent on ϑ_0 and φ_0, while (x_n, y_n) determines the location of the n-th isolated element in the $x - y$ plane.

The second series of the numerator refers to the array pattern of all subarrays, with the l-th subarray pattern denoted by $E_{l,n}(\vartheta, \varphi, \vartheta_0, \varphi_0)$. It is noted that the range of subarray numbering equals $1 \leq l \leq L$ and that the input at the center of the l-th subarray is related to the array index n via $n = N - L + l$. A_l and q_l denote the amplitude and the phase shift factor at the input of the l-th subarray, respectively, the latter also dependent on ϑ_0 and φ_0.

Following further the expression in [42 eqn. (5)], the denominator in (A.2) can be derived into three terms as,

$$\frac{1}{3}\sum_{n=1}^{N} A_n^2 + 2\sum_{n=1}^{N}\sum_{p_{l,m}=1}^{P_{l,n}-1}\sum_{p_{l,n}=p_{l,m}+1}^{P_{l,n}} A_n^2 B_{p_{l,n}}^{(l)}{}^2 B_{p_{l,m}}^{(l)}{}^2$$
$$\times cos(\Delta\psi)\left(\frac{sin(Z_{n,n})}{Z_{n,n}^3} - \frac{cos(Z_{n,n})}{Z_{n,n}^2}\right)$$
$$+ 2\sum_{m=1}^{N-1}\sum_{n=m+1}^{N}\sum_{p_{l,m}=1}^{P_{l,n}-1}\sum_{p_{l,n}=p_{l,m}+1}^{P_{l,n}} A_n A_m B_{p_{l,n}}^{(l)}{}^2 B_{p_{l,m}}^{(l)}{}^2$$
$$\times cos(\Delta\psi + \Delta q)\left(\frac{sin(Z_{m,n})}{Z_{m,n}^3} - \frac{cos(Z_{m,n})}{Z_{m,n}^2}\right) \quad (A.3)$$

In (A.3), the series in the first term covers all the isolated and the subarray center elements, where $B_{p_{l,n}}^{(l)} = 1$ for $n > N - L$. The second term includes the contribution to the radiated power from isolated, center and non-isolated element while taking the mutual coupling in the radiation pattern between center and non-isolated elements into account. In the

third term, the double summations range from $m = 1$ up to $m = N - 1$ and from $n = m + 1$ up to $n = N$. This term describes the mutual coupling between isolated elements and center plus non-isolated elements.

For $n, m \leq N - L$, the amplitudes A_n and A_m denote the amplitudes of the n and m-th isolated elements at locations (x_m, y_m) and (x_n, y_n), respectively. For, $N - L + 1 \leq m$, $m + 1 < n < N$, A_n and A_m are the input amplitudes of the n-th, m-th subarray respectively. As will be explained in the next sub-sections describing different types of subarrays, the phase factors q_n and q_m for subarrays also depend on the subarray configuration integrated in the full array. It should be noted that in the following discussions the numbering of subarrays with center feeding may have one or two values (n or n and $n+1$) for subarrays with one or two feeding inputs, respectively.

REFERENCES

[1] A. Ishimaru, "Unequally spaced arrays based on the Poisson sum formula," *IEEE Trans. Antennas Propag.*, vol. 62, no. 4, pp. 1549–1554, Apr. 2014.

[2] W. P. M. N. Keizer, "Synthesis of thinned planar circular and square arrays using density tapering," *IEEE Trans. Antennas Propag.*, vol. 62, no. 4, pp. 1555–1563, Apr. 2014.

[3] O. M. Bucci, T. Isernia, S. Perna, and D. Pinchera, "Isophoric sparse arrays ensuring global coverage in satellite communications," *IEEE Trans. Antennas Propag.*, vol. 62, no. 4, pp. 1607–1618, Apr. 2014.

[4] J. L. A. Quijano, M. Righero, and G. Vecchi, "Sparse 2-D array placement for arbitrary pattern mask and with excitation constraints: A simple deterministic approach," *IEEE Trans. Antennas Propag.*, vol. 62, no. 4, pp. 1652–1662, Apr. 2014.

[5] G. Oliveri, E. T. Bekele, F. Robol, and A. Massa, "Sparsening conformal arrays through a versatile *BCS*-based method," *IEEE Trans. Antennas Propag.*, vol. 62, no. 4, pp. 1681–1689, Apr. 2014.

[6] P. Angeletti and G. Toso, "Array antennas with jointly optimized elements positions and dimensions part I: Linear arrays," *IEEE Trans. Antennas Propag.*, vol. 62, no. 4, pp. 1619–1626, Apr. 2014.

[7] P. Angeletti, G. Toso, and G. Ruggerini, "Array antennas with jointly optimized elements positions and dimensions part II: Planar circular arrays," *IEEE Trans. Antennas Propag.*, vol. 62, no. 4, pp. 1627–1639, Apr. 2014.

[8] M. C. Vigano, D. Llorens del Rio, F. Bongard, and S. Vaccaro, "Sparse array antenna for ku-band mobile terminals using 1 bit phase controls," *IEEE Trans. Antennas Propag.*, vol. 62, no. 4, pp. 1723–1730, Apr. 2014.

[9] H. Unz, "Linear arrays with arbitrarily distributed elements," *IRE Trans. Antennas Propag.*, vol. 8, no. 2, pp. 222–223, Mar. 1960.

[10] R. Harrington, "Sidelobe reduction by nonuniform element spacing," *IRE Trans. Antennas Propag.*, vol. 9, no. 2, pp. 187–192, Mar. 1961.

[11] A. Maffett, "Array factors with nonuniform spacing parameter," *IRE Trans. Antennas Propag.*, vol. 10, no. 2, pp. 131–136, Mar. 1962.

[12] R. E. Willey, "Space tapering of linear and planar arrays," *IRE Trans. Antennas Propag.*, vol. 10, no. 4, pp. 369–377, Jul. 1962.

[13] A. Ishimaru, "Theory of unequally-spaced arrays," *IRE Trans. Antennas Propag.*, vol. 10, no. 6, pp. 691–702, Nov. 1962.

[14] W. Doyle, "On approximating linear array factors," RAND Corp., Santa Monica, CA, USA, Tech. Rep. Mem RM-3530-PR, Feb. 1963.

[15] R. M. Leahy and B. D. Jeffs, "On the design of maximally sparse beamforming arrays," *IEEE Trans. Antennas Propag.*, vol. 39, no. 8, pp. 1178–1187, Aug. 1991.

[16] D. Caratelli and M. C. Vigano, "A novel deterministic synthesis technique for constrained sparse array design problems," *IEEE Trans. Antennas Propag.*, vol. 59, no. 11, pp. 4085–4093, Nov. 2011.

[17] R. L. Haupt, "Thinned arrays using genetic algorithms," *IEEE Trans. Antennas Propag.*, vol. 42, no. 7, pp. 993–999, Jul. 1994.

[18] D. G. Leeper, "Isophoric arrays-massively thinned phased arrays with well-controlled sidelobes," *IEEE Trans. Antennas Propag.*, vol. 47, no. 12, pp. 1825–1835, Dec. 1999.

[19] G. Oliveri, M. Donelli, and A. Massa, "Linear array thinning exploiting almost difference sets," *IEEE Trans. Antennas Propag.*, vol. 47, no. 12, pp. 1825–1835, Dec. 1999.

[20] M. Skolnik, G. Nemhauser, and J. Sherman, "Dynamic programming applied to unequally spaced arrays," *IEEE Trans. Antennas Propag.*, vol. AP-12, no. 1, pp. 35–43, Jan. 1964.

[21] R. Arora and N. Krisnamacharyulu, "Synthesis of unequally spaced arrays using dynamic programming," *IEEE Trans. Antennas Propag.*, vol. AP-16, no. 5, pp. 593–595, Sep. 1968.

[22] E. Tohidi, M. M. Nayebi, and H. Behroozi, "Dynamic programming applied to large circular arrays thinning," *IEEE Trans. Antennas Propag.*, vol. 66, no. 8, pp. 4025–4033, Aug. 2018.

[23] J. Fondevila-Gómez, A. A. Salas-Sánchez, J. A. Rodríguez-González, and F. J. Ares-Pena, "Density-tapered planar arrays for multibeam and shaped beam coverage in satellite communications," in *Proc. 9th Eur. Conf. Antennas Propag. (EuCAP)*, 2015, pp. 1–5.

[24] X. Zhao, Q. Yang, and Y. Zhang, "A hybrid method for the optimal synthesis of 3-D patterns of sparse concentric ring arrays," *IEEE Trans. Antennas Propag.*, vol. 64, no. 2, pp. 515–524, Feb. 2016.

[25] C. Bencivenni, M. V. Ivashina, R. Maaskant, and J. Wettergren, "Synthesis of maximally sparse arrays using compressive sensing and full-wave analysis for global Earth coverage applications," *IEEE Trans. Antennas Propag.*, vol. 64, no. 11, pp. 4872–4877, Nov. 2016.

[26] X. Zhao, Y. Zhang, and Q. Yang, "Synthesis of sparse concentric ring arrays based on Bessel function," *IET Microw., Antennas Propag.*, vol. 11, no. 11, pp. 1651–1660, Sep. 2017.

[27] O. M. Bucci, S. Perna, and D. Pinchera, "Interleaved isophoric sparse arrays for the radiation of steerable and switchable beams in satellite communications," *IEEE Trans. Antennas Propag.*, vol. 65, no. 3, pp. 1163–1173, Mar. 2017.

[28] A. A. Salas-Sanchez, J. A. Rodriguez-Gonzalez, and F. J. Ares-Pena, "Hybrid method for the synthesis of isophoric phase-shaped beams," *IEEE Trans. Antennas Propag.*, vol. 66, no. 12, pp. 7439–7442, Dec. 2018.

[29] D. Pinchera, M. D. Migliore, and G. Panariello, "Synthesis of large sparse arrays using IDEA (inflating-deflating exploration algorithm)," *IEEE Trans. Antennas Propag.*, vol. 66, no. 9, pp. 4658–4668, Sep. 2018.

[30] D. Dai, M. Yao, H. Ma, W. Jin, and F. Zhang, "An effective approach for the synthesis of uniformly excited large linear sparse array," *IEEE Antennas Wireless Propag. Lett.*, vol. 17, no. 3, pp. 377–380, Mar. 2018.

[31] A. Kedar, "Deterministic synthesis of wide scanning sparse concentric ring antenna arrays," *IEEE Trans. Antennas Propag.*, vol. 67, no. 12, pp. 7387–7395, Dec. 2019.

[32] D. Caratelli, G. Toso, O. V. Stukach, and N. V. Panokin, "Deterministic constrained synthesis technique for conformal aperiodic linear antenna arrays—Part I: Theory," *IEEE Trans. Antennas Propag.*, vol. 67, no. 9, pp. 5951–5961, Sep. 2019.

[33] D. Caratelli, G. Toso, O. V. Stukach, and N. V. Panokin, "Deterministic constrained synthesis technique for conformal aperiodic linear antenna arrays—Part II: Applications," *IEEE Trans. Antennas Propag.*, vol. 67, no. 9, pp. 5962–5973, Sep. 2019.

[34] J. S. Herd, S. M. Duffy, and H. Steyskal, "Design considerations and results for an overlapped subarray radar antenna," in *Proc. IEEE Aerosp. Conf.*, Big Sky, MT, USA, Mar. 2005, pp. 1087–1092.

[35] R. L. Haupt, "Optimized weighting of uniform subarrays of unequal sizes," *IEEE Trans. Antennas Propag.*, vol. 55, no. 4, pp. 1207–1210, Apr. 2007.

[36] T. Azar, "Overlapped subarrays: Review and update," *IEEE Antennas Propag. Mag.*, vol. 55, no. 2, pp. 228–234, Apr. 2013.

[37] D. Petrolati, P. Angeletti, and G. Toso, "A lossless beam-forming network for linear arrays based on overlapped sub-arrays," *IEEE Trans. Antennas Propag.*, vol. 62, no. 4, pp. 1769–1778, Apr. 2014.

[38] F. S. Akbar, L. P. Ligthart, I. E. Lager, and G. Hendrantoro, "Subarrays in linear array configurations, an effective instrument for scan loss compensation," in *Proc. Loughborough Antennas Propag. Conf. (LAPC)*, Nov. 2016, pp. 1–5.

[39] F. S. Akbar, L. P. Ligthart, G. Hendrantoro, and I. E. Lager, "Scan loss mitigation via subarrays a full-scale concept demonstrator," in *Proc. 47th Eur. Microw. Conf. (EuMC)*, Oct. 2017, pp. 156–159.

[40] F. S. Akbar, L. P. Ligthart, G. Hendrantoro, and I. E. Lager, "Use of subarrays in linear array for improving wide angular scanning performance," *IEEE Access*, vol. 7, pp. 135290–135299, 2019.

[41] C. A. Balanis, *Antenna Theory: Analysis and Design*, 4th ed. New York, NY, USA: Wiley, 2016.

[42] L. P. Ligthart, "A new numerical approach to planar phased arrays," in *Proc. 5th Eur. Microw. Conf.*, Hamburg, Germany, Oct. 1975, pp. 453–457.

[43] B. Rupakula, A. H. Aljuhani, and G. M. Rebeiz, "Limited scan-angle phased arrays using randomly grouped subarrays and reduced number of phase shifters," *IEEE Trans. Antennas Propag.*, vol. 68, no. 1, pp. 70–80, Jan. 2020.

FANNUSH S. AKBAR (Student Member, IEEE) received the B.A.Sc. degree in telecommunication engineering from Politeknik Elektronika Negeri Surabaya, Surabaya, Indonesia, in 2013. He is currently pursuing the Ph.D. degree in electrical engineering with the Institut Teknologi Sepuluh Nopember, Surabaya. His recent research interests include phased-array antenna with wide-angular scanning capability, array synthesis, and microstrip antennas.

L. P. LIGTHART (Life Fellow, IEEE) was born in The Netherlands in 1946. He received the degree *(cum laude)* in engineering and the Ph.D. degree from the Delft University of Technology, and the Honorary doctorate degrees from MSTUCA, Moscow, Tomsk State University, and MTA Romania. Since 1988, he has been the Chair on MW transmission, remote sensing, radar, and positioning and navigation with the Delft University of Technology. He founded the IRCTR at the Delft University of Technology. He is currently an Emeritus Professor with the Delft University of Technology, a Guest Professor with universities in Indonesia and China. He gives various courses on radar, remote sensing, and antennas. He has supervised over 50 Ph.D. students. He has authored or coauthored over 650 articles, various book chapters, and books. His areas of specialization include antennas and propagation, radar and remote sensing, and satellite, mobile, and radio communications. He is a Fellow of the IET and an Academician of the Russian Academy of Transport. He is the Chairman of CONASENSE and a member BoG of IEEE-AESS. He is a Founding Member of the EuMA. He was the Chair of the 1st EuMW in 1998 and has initiated EuRAD in 2004.

GAMANTYO HENDRANTORO (Senior Member, IEEE) was born in Jombang, Indonesia, in 1970. He received the B.Eng. degree from the Institut Teknologi Sepuluh Nopember (ITS), Surabaya, Indonesia, in 1992, and the M.Eng. and Ph.D. degrees from Carleton University, Ottawa, ON, Canada, in 1997 and 2001, respectively, all in electrical engineering. He is currently a Professor with the Department of Electrical Engineering, ITS. He has been engaged in various studies, including investigation into millimeter-wave propagation, channel modeling and wireless systems for tropical areas, studies on HF skywave channels and communications in equatorial regions, and the development of radar array and signal processing. His current research interests include radio propagation channel modeling and wireless communications.

• • •